SOLUTE DISTRIBUTION ANALYSIS IN DIRECTIONALLY SOLIDIFIED Al-5.7 wt% Ni EUTECTIC ALLOY
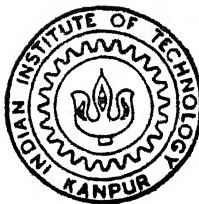
by

V. PRABHAKAR RAO

DEPARTMENT OF MATERIALS AND METALLURGICAL ENGINEERING

INDIAN INSTITUTE OF TECHNOLOGY KANPUR

March 1994

SOLUTE DISTRIBUTION ANALYSIS IN DIRECTIONALLY SOLIDIFIED Al-5.7 wt% Ni EUTECTIC ALLOY

A Thesis Submitted
In Partial Fulfilment of the Requirements
for the Degree of

M. Tech

By

V. PRABHAKAR RAO

to the

DEPARTMENT OF MATERIALS & METALLURGICAL ENGINEERING

INDIAN INSTITUTE OF TECHNOLOGY KANPUR

March, 1994

CERTIFICATE

This is to certify that this work "Solute distribution analysis in directionally solidifi ed Al-5.7 wt% Ni eutectic alloy" has been carried out by Mr V. Prabhakar Rao under our guidance and has not been submitted else where for a degree.

(Dr V. Bansal)
Associate Professor,
Department of Materials
and Metallurgical Engg.,
I I T - KANPUR.

(Dr M. N. Shetty)
Professor,
Department of Materials
and Metallurgical Engg.,
I I T - KANPUR.

March, 1994.

ABSTRACT

Controlled solidification experiments were carried out on Al − 5.7 wt% Ni eutectic alloys to investigate the solute distribution in both longitudinal and transverse directions. Metallography, SEM and scanning electron microprobe were utilised to study the resulting microstructures and solute distributions. For this, the events at the solid − liquid interface are frozen by rapidly quenching in liquid Nitrogen a partially directionally solidified ingot. Jackson and Hunt's analysis for lamellar eutectics is modified for rod morphology to estimate the solute distribution ahead of the solid − liquid interface. The observations ~~are~~ seem to be in good agreement with the experimental results provided a best fit choice is made for the interface diffusion coefficient.

ACKNOWLEDGEMENTS

CONTENTS

LIST OF FIGURES

LIST OF TABLES

CHAPTER 1

INTRODUCTION

A composite material can be described as a mixture of component materials designed to meet a specific engineering role by exploiting the desirable properties of the components, whilst minimising the harmful effects of their less desirable properties. In-situ composites are metal matrix composites, where both matrix and reinforcement are formed during solidification, produced by the directional solidification (DS) of eutectic alloys. Here the reinforcement can be lamellar, fibrous, broken lamellar or spiral depending on the nature of the material dealt with. It has been found that alloys with considerably off eutectic compositions also solidify in the same manner provided the required temperature gradient(G_L) and freezing rate (R) are imposed. Therefore, DS is one of the important routes for producing composites. Directional solidification is a process in which heat is extracted unidirectionally from the molten alloy leading to the orientation of second phase particles parallel to the direction of heat extraction. We cannot get unidirectionally oriented second phase particles and hence anisotropy in mechanical properties in conventional solidification, as heat is extracted out from all directions leading to the formation of small packets of eutectic phase oriented randomly(equiaxed). There are two rules to be followed to avoid equiaxed grain nucleation in the liquid. The melt temperature must be maintained above the liquidus and effective nucleating substrates must be removed from the melt.This explains the effect of impurities on the

structure of directionally solidified alloys. DS can be achieved by slowly lowering the molten charge chilled at one end (often done by copper block) through a stationary furnace of proper thermal gradient, or by slowly withdrawing the furnace from a stationary molten charge chilled as before. The latter technique is advantageous as the molten material will not be subjected to mechanical agitation during solidification and hence no effect on the morphology obtained after DS. This creates a substantially uniaxial heat flow and a planar solid-liquid(S-L) interface normal to the direction of heat extraction for composites where both phases are of the non-faceting type.

Directionally solidified alloys,due to the orientation of second phase particles parallel to the direction of solidification, have reduced tendency for intercrystalline fracture at high temperature arising from excessive creep, creep rupture and thermal fatigue. Fracture in such alloys[1] is found to take place by shear failure of the columnar grain structure or due to the failure of the aligned rods of the second phase.

Some of the important properties of directionally solidified structures are [2],

(a) Permanent magnets with oriented structures,

(b) Superior thermal shock properties,

(c) High strength in the direction of solidification.

The above properties result from,

(a) Improved distribution of second phase particles,

(b) Preferred crystallographic textures,

(c) Reduced microporosity,

(d) Uniformity in microsegregation compared to the conventionally solidified material.

The disadvantages are,

(a) High cost,

(b) Difficult processing methods,

(c) Higher creep rates at intermediate temperatures [3],

(d) Slow and controlled rate of solidification,

(e) Fixed volume fraction of reinforcement,

(f) Fixed configuration of reinforcement.

Directionally solidified alloys are used at least in these different areas,

(a) For many room temperature applications requiring improved properties particularly resistance to fracture,

(b) In production of high temperature turbine blades and super conductors [4,5,6],

(c) In production of hard magnetic materials.

As we know solute diffusion plays an important role in the solidification of alloys. Freezing in pure metals is a heat flow problem, but in eutectic alloys , it is a heat and mass flow problem. In single phase alloys the solute diffusion is important generally in the direction of solidification. In polyphase lamellar and rod eutectic alloys for example an added degree of complication arises from the fact that solute has to diffuse both transverse to and along the growth direction resulting in phase separation. The growth of the phases is then determined by the local constraints that exists at S-L interface during growth, which in turn governs the size and volume distribution of these phases. In the present

work our main aim is to examine the solute distribution at the S-L interface in a directionally solidified eutectic alloy. We have chosen the Al-5.7 Wt% Ni eutectic alloy with a melting point of $640^{\circ}C$ and in which the Al_3Ni (β) phase with 42 wt% Ni grows as rods in the Al rich α-phase matrix containing negligible concentration of Ni(0.05 wt%). In a directionally solidified alloy these rods normally get aligned along the direction of freezing surrounded by the Al matrix, thus providing an ideal system for examining solute properties both in and around the rod spaces. The S-L interface is observed by instantaneously quenching a partly directionally solidified alloy in liquid nitrogen(LN_2). The solute distribution in and around the interrod spaces near the arrested S-L interface is determined by scanning electron microprobe analysis(SEMPA) and compared with the theoretical profiles from the diffusion equation.

CHAPTER 2

LITERATURE REVIEW

The literature review is done under the following four broad categories.

(2.1) Heatflow, Unidirectional solidification and techniques,

(2.2) Eutectic solidification and growth characteristics,

(2.3) Directional solidification and mechanical properties,

(2.4) Directional solidification and magnetic properties.

(2.1) Heat flow, Unidirectional solidification and techniques:

(2.1.1) Heat flow:

Controlled heat extraction in one direction from the freezing alloy is a requirement to achieve DS. This takes place effectively if the heat is extracted at the mold-metal interface unidirectionally through one plane which can be caused by using an efficient metallic chill. Often this is done by providing a copper chill at the bottom end of a crucible containing the melt, resulting in DS anti parallel to the direction of heat extraction. If necessary water can be passed through the chill to increase its chilling efficiency. The chill used must have the following properties,

(a) It must have high thermal conductivity to conduct the sensible heat out of the system. A copper chill meets this requirement.

(b) The surface of the chill must be cleaned before each casting

run by removing any oxidised layer at the crucible-chill interface so that resistance to heat flow is minimised.

(c) There should be good contact between the chill and the crucible.

In spite of all these, heat transfer can occur through convection in in the melt all directions which will affect the continuity and alignment of the second phase particles and thus weakening the structure. Convection takes place because of thermal and concentration gradients together with the gravitational force in the liquid metal.

Thus for a good DS a perpendicular arrangement of crucible containing the melt with a continuously rising G_1 to the top of the crucible is a necessary requirement. The convection can also be kept to a minimum by not resorting to induction methods of heating.

(2.1.2) Unidirectional solidification:

DS of multicomponent eutectics is satisfactorily accomplished by maintaining a planar growth front and fulfilling the following conditions [7].

(a) Unidirectional heat flow from the melt and no convection current within the melt,

(b) No nucleation ahead of the S-L interface. This can be taken care of by maintaining a G_L above the liquidus temperature ahead of the growth front and as far as possible avoiding the impurity particles in the melt,

(c) $\left[\dfrac{G_L}{R} \right] > 0$, where,

G_L -is the temperature gradient in the liquid at the S-L interface and R-is the growth velocity.

(2.1.3)Experimentaltechniquesfor directional solidification:

There are several techniques known for controlling heat transfer to provide unidirectional solidification.

(2.1.3.1) Mold is sufficiently insulated so that after the molten metal is cast most of the heat flow takes place through some bottom chill. The chill could be a liquid metal having sufficiently low vapor pressure. Since liquid superheat is rapidly lost via conduction to the chill face it must be replenished as growth continues, by adding it externally.

It is essential that the mold be in a vertical position so that S-L interface advances in a predominantly horizontal plane, which reduces the convective fluid motion and radial heat transfer usually associated with a vertical S-L interface. As the melt superheat gradually dissipates, the temperature gradient in the liquid gradually decreases until nucleation takes place in the liquid ahead of the S-L interface and columnar growth ceases. A major problem with this casting method is that both solidification rate and temperature gradient decrease with distance from the chill,thus causing deterioration in mechanical properties along the length of the ingot.

(2.1.3.2) Controlling heat transfer rate by an external power source:

(2.1.3.2.a) "Power down growth control method", in which heat transfer rate is controlled by gradually lowering the power in the furnace that surrounds a fixed mold. For high melting alloys, this method is generally adopted.

In the power down technique, an open ended mold is attached to a water cooled copper chill and placed in two zone induction coil, coupled by a graphite susceptor for heating. The superheated alloy is poured to the hot mold having an established temperature profile above the melting point of the alloy due to energising the induction coils.

After holding the alloy for sometime for equilibration purpose, the bottom coil is turned off and directional solidification is allowed to proceed in the axial temperature gradient. Since the S-L interface moves away from the chill surface solidification rate decreases, with structural variations at the top of the ingot.

(2.1.3.2.b) "High rate solidification method" (generally adopted for high melting alloys), in which heat transfer rate is controlled by withdrawing the mold and maintaining the power source in a fixed position.

The high rate solidification is essentially an improvement on the power down method permitting efficient directional heat transfer. Here the crucible attached as before is withdrawn from a single zone induction heating through a radiation baffle, which helps to maintain a uniform temperature with in the heated zone by preventing any radiation losses. This method is know to produce a much more refined micro structure.

(2.1.3.2.c) "The Bridgeman Stockberger method", is used for low melting alloys. Heat transfer rate is controlled either by moving the heat source(furnace) keeping the mold(crucible) in a fixed position or by lowering the mold through the fixed heat

source(the later technique is used in the present investigation). This method can almost eliminate the variable structure disadvantage of the Power down technique. This technique has the advantage that the environment during freezing remains constant throughout a large portion of freezing cycle. Columnar castings can be solidified almost four times faster with this method than with Power down technique.

(2.2) Eutectic solidification and growth charecteristics:

(2.2.1)Eutectic morphology:

From experimental observations, single phase materials can be divided into two groups according to their solidification characteristics. Those that grow as non faceted and others as faceted crystals. Jackson[8] showed that type of growth depends on a factor α which is almost the entropy of melting and given by the relation [9]

$$\alpha = \frac{L_m . W}{K . T_m} \qquad (2.1)$$

Where L_m - is latent heat of melting,

K - is Boltzman constant,

W - is crystallographic factor,

T_m - is melting point.

Most metals have α<2 and grow with no facets, i.e. rough interface. Based on this eutectics can be classified as,

(2.2.1.a) Rough-Rough: (α<2 for both the phases)

Al-Ni, Al-Zn,Al-Cu and most of the metallic alloys come under this category.They can have one of the following microstructures.(i) Lamellar (ii)Rod (iii)Cellular

or Colony. Cellular or Colony morphology is obtained when there is a third element as impurity. Because this brings supercooling ahead of the interface and thus planar interface breaks down into cellular.

(2.2.1.b) Rough-Faceted: (α<2 for one face and α>2 for the other) Al-Si(Al-rough,Si-faceted), Fe-Graphite [10]come under this classification.

(2.2.1.c) Faceted-Faceted: (α>2 for both the phases)

Organic compounds grow in this way. Since our present work deals with Al-Ni system it is necessary to understand why Al-Ni system has rod morphology.

For eutectic alloys, when precipitating phase has a low volume fraction there is a tendency to form rods and for high volume fraction the tendency is to form lamellae. It is generally accepted that interfacial energy is the driving force for the formation of either of the morphologies although in some cases solidification variables(R,G_l etc) can influence the morphology. The surface area(S_r) associated with a fibrous system is very much sensitive to the volume proportions rising from zero to a maximum of 0.8 when the rods would tend to make contact. On the other hand, the surface area of lamellar array(S_l)is independent of volume fraction since it is independent of lamellar thickness. The preference for a given habit as determined by simple geometric considerations is shown in Fig 2.1. The critical volume fraction (V_f) at which rod morphology changes to lamellar has been found to be approximately 0.3 .
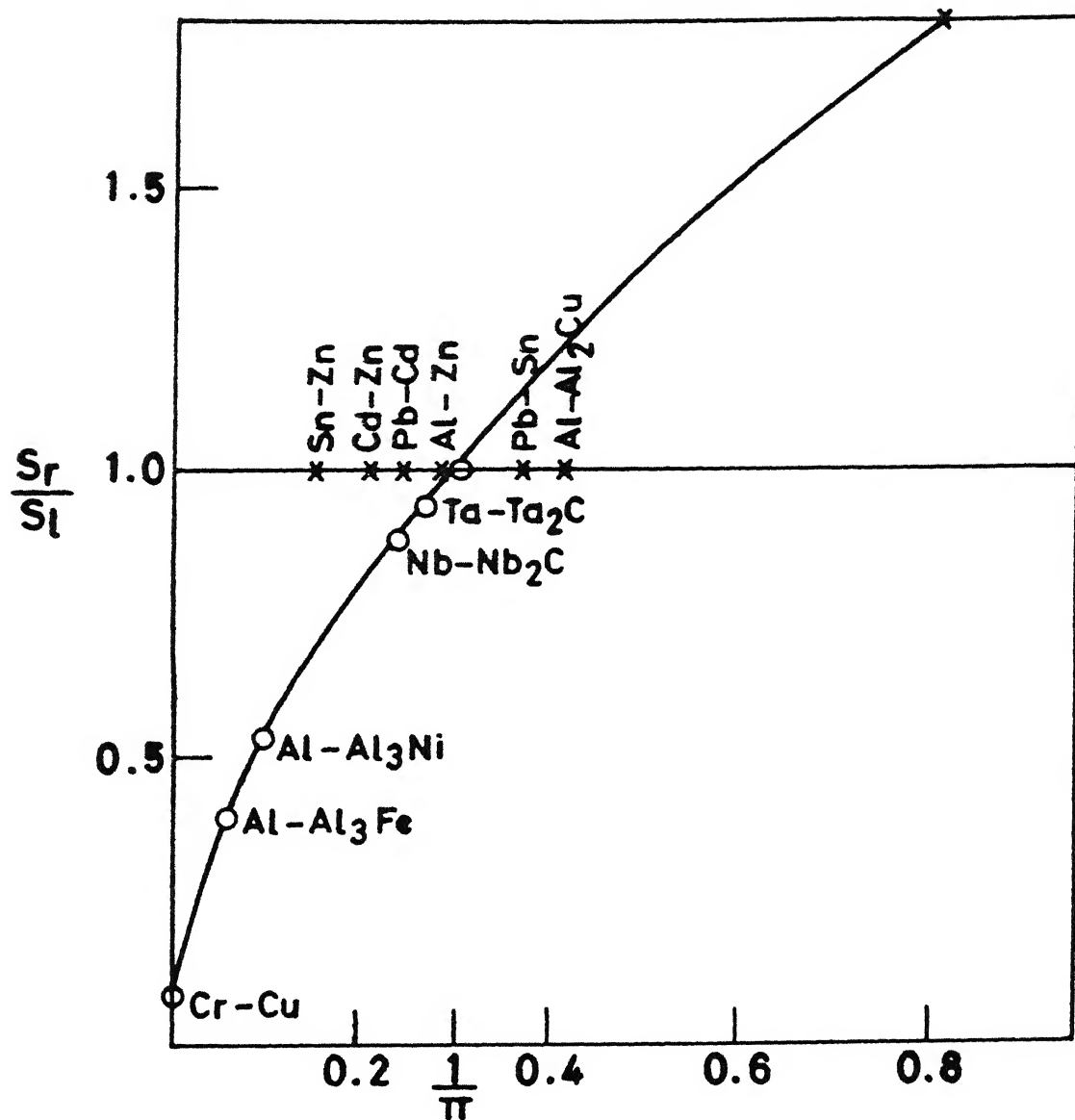
Fig.2.1 The relative surface areas for lamellar eutectic arrangements(s_l),compared with those of rods(s_r), as functions of volume fractions.

(2.2.2) Mechanism of eutectic growth:

The mechanism of eutectic growth in non faceted alloys has been treated in a simplified manner by Jackson and Hunt[11] for lamellar morphology. Consider an alloy of eutectic composition (C_E) as in Fig 2.2(a), growing with a plane front except that the individual lamellae have slightly curved interfaces as sketched in Fig 2.2(b). As α phase grows it rejects B atoms into the liquid. Similarly the growing β phase rejects A atoms. Thus there is a slight build up of A atoms in front of α lamellae and depletion in front of the β lamellae as shown in Fig 2.3(a). If equilibrium pertains at the S-L interface there must now be an undercooling in front of the lamellae which depends on the amount of solute build up or depletion. This under cooling is,

$$\Delta T_D = T_E - T_L = m_L \cdot \left[C_E - C_0 \right] \qquad (2.2)$$

Where,

ΔT_D - is under cooling due to solute diffusion,

m_L - is liquidus slope,

C_L^* - is composition of the liquid at the location y on the S-L interface.

ΔT_D is marked on the phase diagram in Fig 2.2(a) for a specific location y_1 in front of the α lamellae and shown schematically in Fig 2.2(b) with respect to y. It is noted that ΔT_D can be positive or negative depending on the actual value of C_L^*. Here the interface temperature T^* is assumed to be constant as shown in Fig 2.3(b). This must be true for the non faceted eutectics because the curved surfaces of lamellae in these eutectics usually deviate from a plane by less than a few
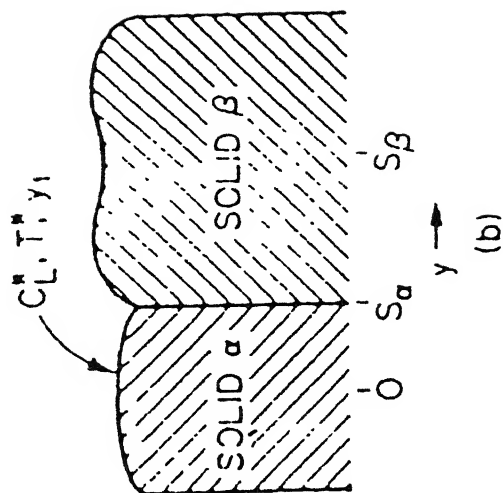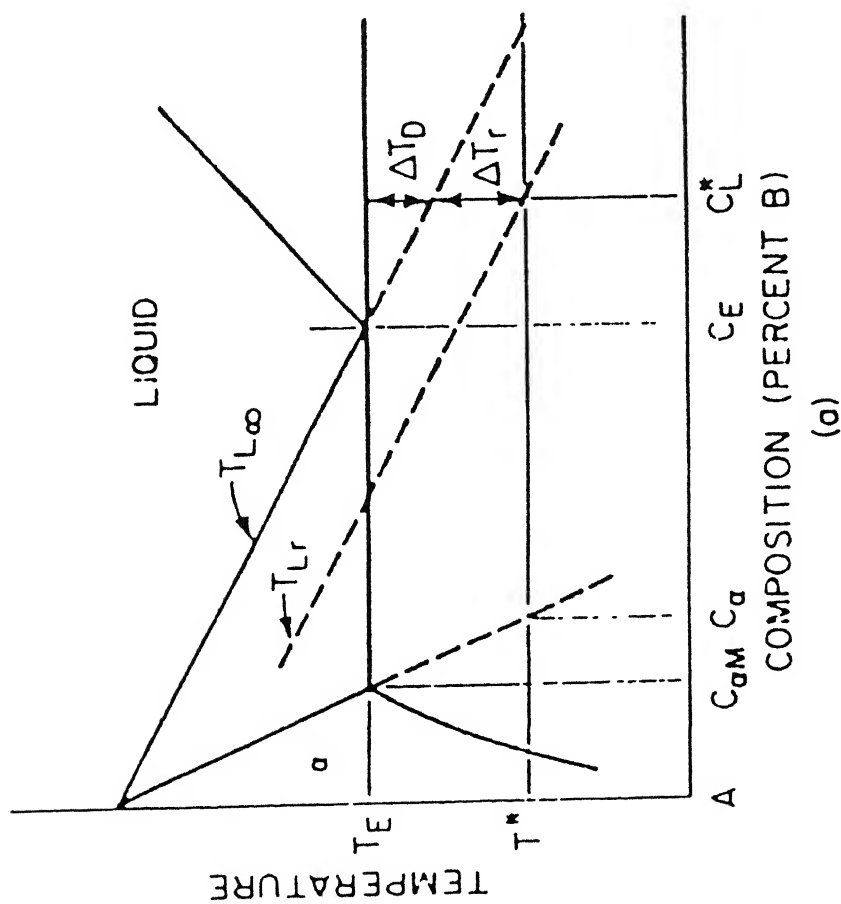
Fig.2.2 Undercooling and interface liquid composition C_L^* of a eutectic alloy at a point on the interface infront of the phase, (a) phase diagram, (b)Interface showing point y_1 for construction of (a) applies.

(a)

COMPOSITION, C_L^*

C_E

(b)

TEMPERATURE

T_E

ΔT_D

ΔT_r

ΔT_D

ΔT_r

ΔT

T^*

$Y \longrightarrow$

B RICH-LIQUID   A RICH-LIQUID

SOLID α SOLID β

0   S_α S_β

(c)
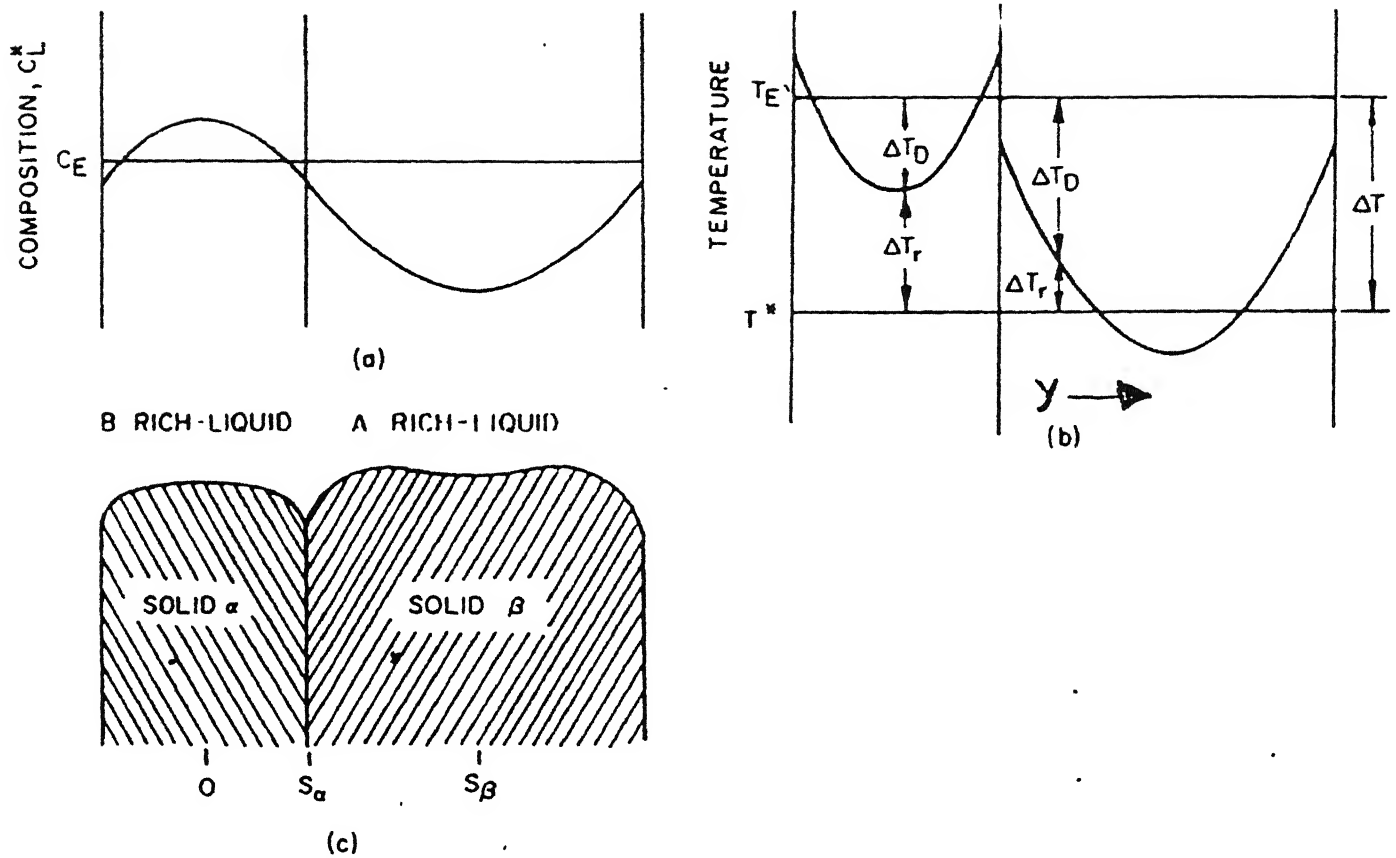
Fig.2.3 Lamellar curvature in eutectic growth (a) Solute concentration in the liquid at the interface, (b) Interfacial undercoolings ΔT_r, ΔT_D and ΔT, (c) Predicted shape of the lamellar solid -liquid interface.(From Hunt and Jackson)

microns. Hence even if the temperature gradient exits in the growth direction, the variation in the temperature from the leading to lagging part of the lamellae is negligible. The interface is maintained isothermal at temperature T^* by the lamellae adjusting their radii of curvature locally. Then the total under cooling at the interface,ΔT,is constant Fig 2.3(b) and is given by;

$$\Delta T = T_E - T^* \qquad (2.3)$$
$$= \Delta T_D + \Delta T_r$$

Where,

$$\Delta T_r = T_{L\infty} - T_{Lr} \qquad (2.4)$$

ΔT_r -is undercooling due to radius of curvature,

T_{Lr}- is liquidus temperature of singly curved surface of radius r.

Fig 2.2(a) shows this depression of liquidus temperature at a location y_1 on the interface of the α phase of a growing eutectic. The interface shape shown in Fig 2.3(c) is that which produces the required values of ΔT_r along the interface. In case of rod morphology both the radii of curvature are to be taken into consideration.

(2.2.3) Mechanism of alternate layer formation:

Tiller[12] proposed a mechanism for alternate layer formation. The basic principle behind this mechanism is that the two phases (α,β) nucleate at different undercooling. If a melt of eutectic composition is cooled at some degree of supercooling nuclei of one phase will form in the liquid. As the crystals of this phase begin to grow, change in

solute content in the vicinity of the growing crystal takes place further under cooling the interface with respect to the second phase. The initial nuclei will probably grow as rods or plates as shown in Fig 2.4(a). If the primary phase serves as an effective nucleus for the second phase, the second phase will nucleate on the surface of the primary phase and obsorbs the super cooling. Fig 2.4(b) illustrates this.

(2.2.4) Interspacing adjustments:

ΔT, R and λ for directionally solidified lamellar and rod eutectic are related by [12];

$$\Delta T = AR\lambda + B/\lambda \qquad (2.5)$$

Where,

ΔT - is undercooling,

R - is growth velocity,

λ - is interlamellar or interrod spacing, and A & B are constants which are functions of the alloy system under consideration.

For a fixed R, ΔT, λ can have a series of values and is plotted in Fig 2.5. Experimental data however show no such ambiguity that is for each R, a particular λ is obtained [13]. The simplest explanation for this is that the growth takes place at the extremum(m) i.e. at minimum undercooling for a given R or equivalently maximum velocity for a given undercooling as shown in Fig 2.5. With this background differentiation of equation(2.5) gives;

$$\lambda^2 R = B/A = constant. \qquad (2.6)$$

Substituting the value of 'R' from (2.6) in to (2.5) leads to;

$$\frac{\Delta T^2}{R} = 4AB = constant. \qquad (2.7)$$

(a)

(b)
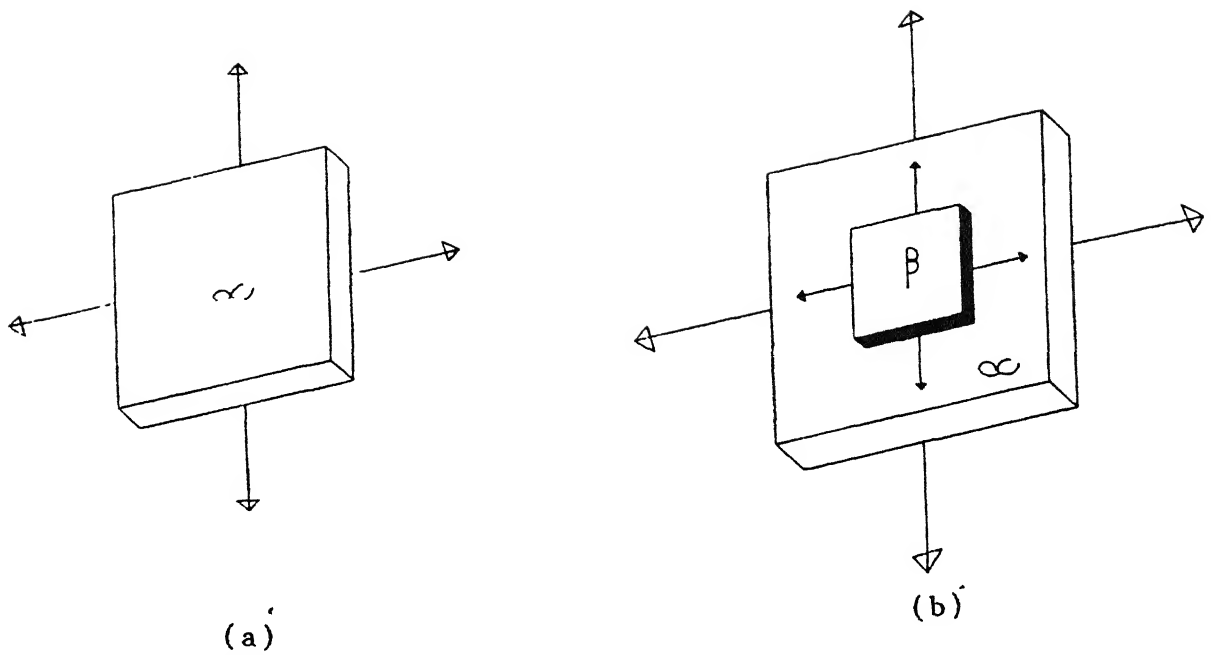
Fig.2.4 Mechanism of alternate layer formation (a) Primary phase particle (b) Nucleation of secondary phase.
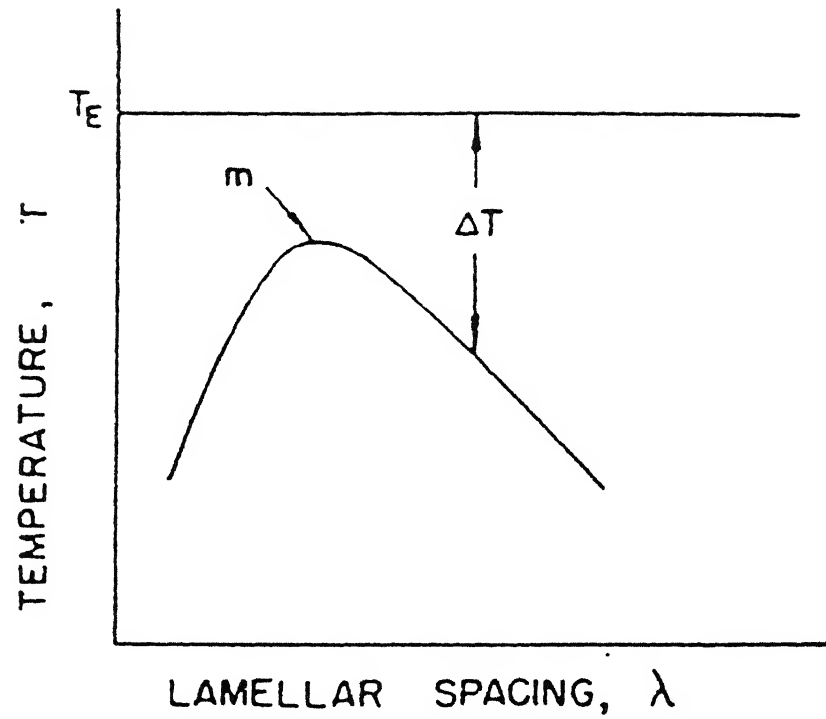
Fig.2.5 Change of interface temperature with lamellar spacing at constant growth rate.

Several measurements [14,15,16] have been done to confirm the fact that growth occurs close to the extremum condition. The results of one of such experiments on Al-CuAl$_2$ eutectic system has been shown in Fig 2.6. The figure shows the calculated growth curves for Al-CuAl$_2$ eutectic alloy and the position of the experimental point for different growth velocities.

There were also attempts to verify the relation between interlamellar or interrod spacing and growth velocity. Lemkey *et al.*[17] and Livingston *et al.*[18] have tried to verify the relation $\lambda^2 R$ = constant for Al-Al$_3$Ni eutectic system. The results of the experiment is shown in Fig 2.7. The solid points on the plot are from Lemkey *et al.* and open points from Livingston *et al.* Chadwick [19], Davis [20] and Mollard [21] have verified the same result for Sn-Pb system. The results are shown in Fig 2.8.

(2.2.5) Development of preferred orientation:

The interfacial energy $\sigma_{\alpha\beta}$ will depend upon the orientation of the $\alpha-\beta$ interface plane. The S-L interface is a sensitive function of $\sigma_{\alpha\beta}$ which leads to a preferred orientation of the columnar axis of the eutectic grains. Fig 2.9 represents a bicrystal growing at some velocity 'V'. The right hand grain has an orientation such that the preferred interface between lamellae is perpendicular to the S-L interface. If the lamellae boundaries follow the preferred plane, the lamellae in the left crystal are growing edgewise at the rate $V' = \dfrac{V}{\cos\phi}$ and the interface undercooling is greater for left hand side grain [equation(2.7)] than the right. Since right
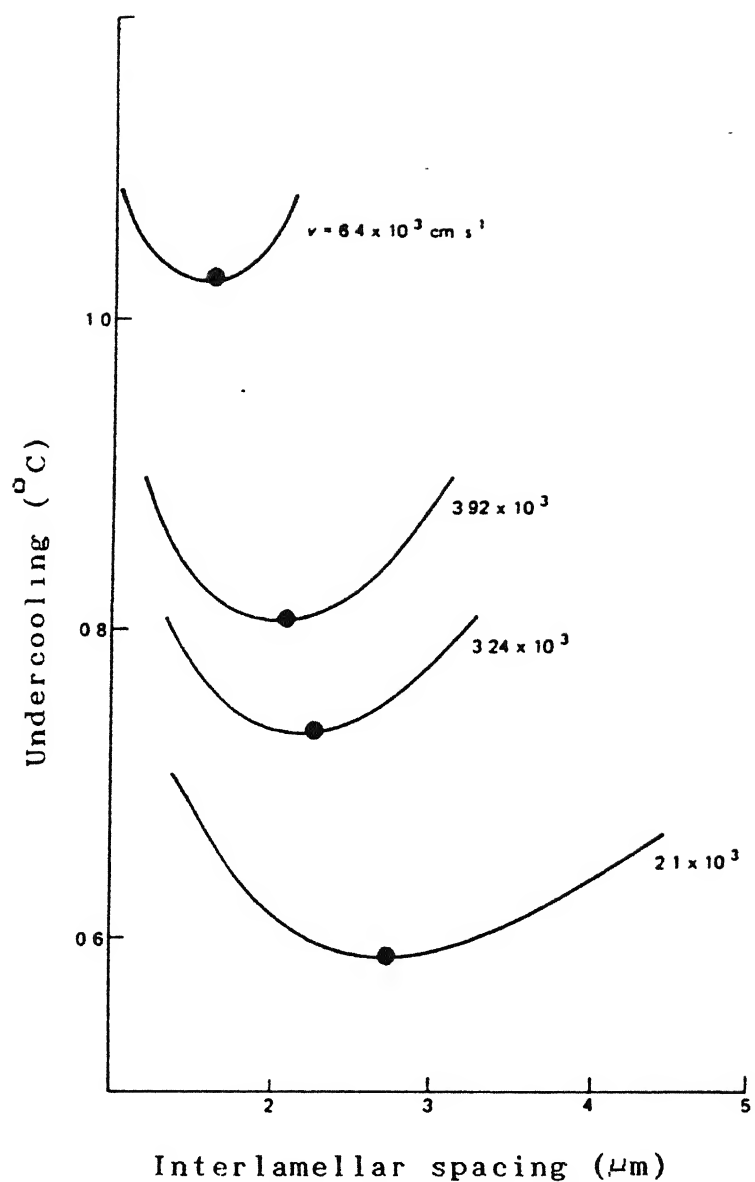
Fig.2.6 The calculated growth curves for Al-CuAl$_2$ eutectic alloy and the position of the experimental point for different growth velocities.
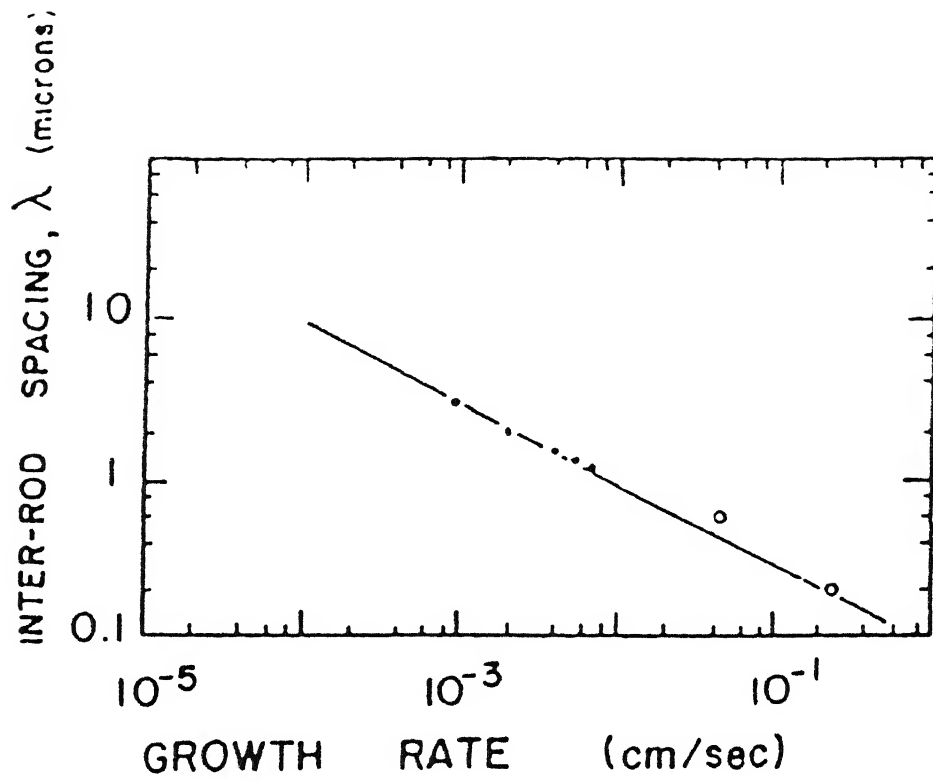
Fig.2.7 Interrod spacing of Al-Al$_3$Ni eutectic (Solid points are from Lemkey et al. and open points from Livingston et al.)
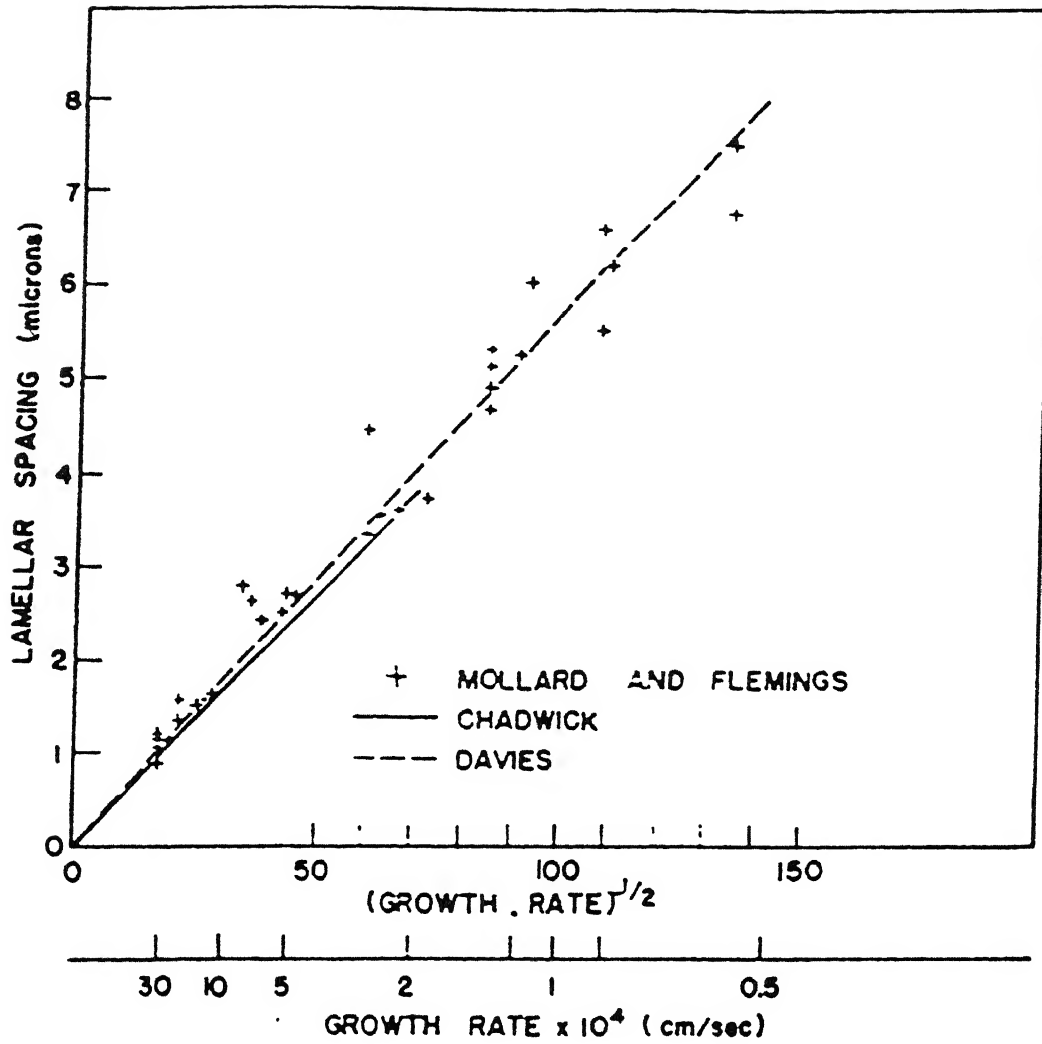
Fig.2.8 Lamellar spacing as a function of growth rate; Tin- Lead composites.(Results of Chadwick and Davies are for eutectic composition. Points from Mollard and Flemings are of off eutectic alloys).
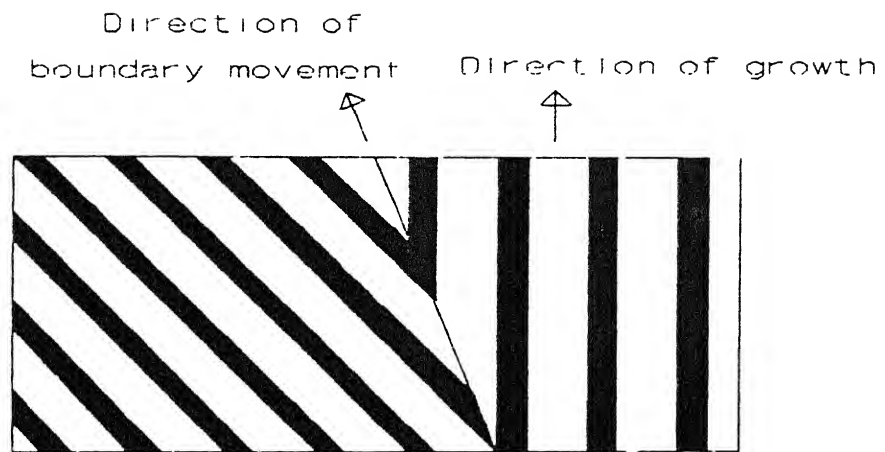
Fig.2.9 Development of preferred orientation of columnar grains.

grain can grow at lower undercooling than the left it is favoured resulting in the elimination of the left grain. In the final structure the surviving grains will be those having preferred $\alpha-\beta$ plane parallel to the specimen axis.

(2.2.6) **Mechanisms of interlamellar spacing adjustments:**

There have been several mechanisms proposed as to how lamellae adjust their spacings when there is a change in growth rate. The following two mechanisms are important for discussion.

(2.2.6.a) **New lamellae formation in the pocket of the other phase:**

Jackson & Hunt [22] have shown that spacings smaller than that at the extremum are inherently unstable. Thus the extremum spacing is expected to be the minimum observed. Spacings some what larger than the extremum are not obviously unstable, but when they become very much larger(a factor of 2 or more), interface curvature can no longer maintain an isothermal interface. Then a pocket develops as shown in Fig 2.10(a) in one phase and drops progressively back from the interface until the growth of the other occurs in it. When this occurs the spacing is abruptly reduced by a factor of 2. This abrupt change in spacing is observed in thin-section transparent organics when growth rate is gradually increased and in bulk specimens when growth rate is abruptly increased by a large amount. But, later experimental results showed that bulk specimens also do exhibit changes in spacing for relatively small changes in growth rate. This fact was the reason for the following additional mechanism.
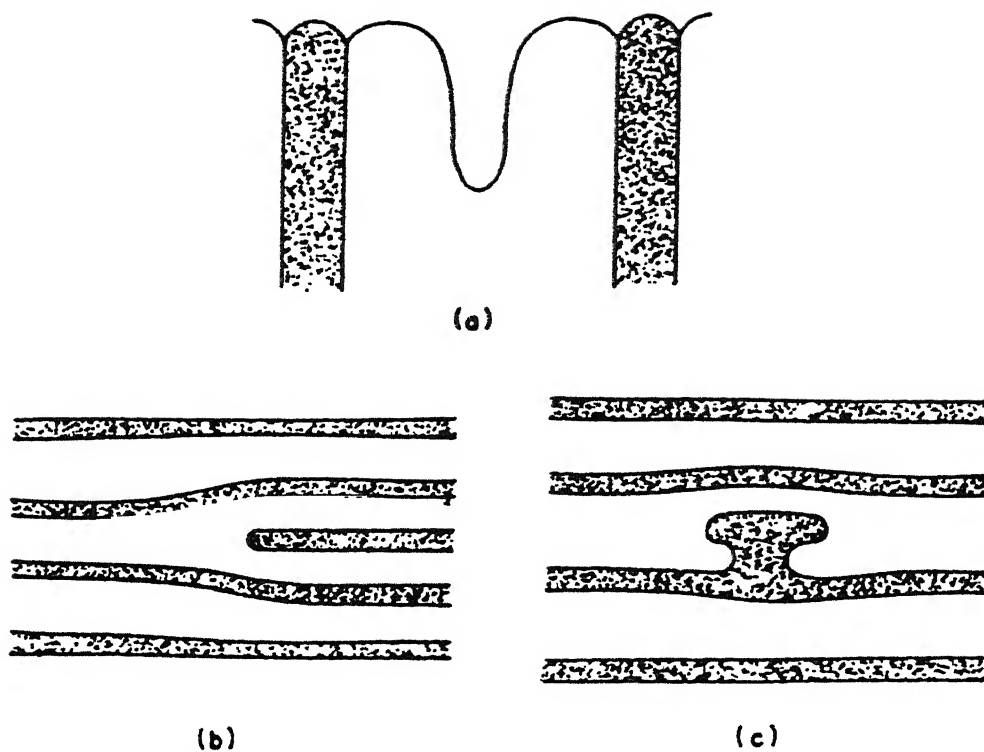
Fig.2.10 Schematic illustrations of mechanisms where by plate spacing adjusts to increasing growth rate, (a) New lamellae form in a pocket of the wide phase, (b) Extra lamellae move left, (c) A plate branches and new lamellae move left and right. In (a) growth direction is upward in the plane of the paper;In (b) and (c) it is perpendicular to the plane of the paper.

(2.2.6.b) Lateral movement of terminations:

This mechanism was first proposed by Jackson & Chalmers [23] and then developed by Hunt & Jackson [24]. According to them the lamellar spacing adjustment takes place because of the lateral movements of the terminations as shown in Fig 2.10(b). These lamellar terminations may be present in the structure or may be formed by plate branching [25] as shown in Fig 2.10(c). A local perturbation caused an incipient lamellae to form as the interface progresses. As shown in Fig 2.10(b), the average spacing to the left of the termination is larger than that to the right and if the termination moves left ward during growth, overall average spacing is decreased. If it moves to the right, average spacing is increased. Now, suppose the lamellar spacing to the left of the termination is larger than that of the extremum(m) then it will be growing at a larger undercooling than that portion to the right o the termination. A slight depression will form in the interface to the left of the termination at this point and the termination will move left ward. The result is that the overall undercooling of the interface is reduced.

(2.3) Directional solidification and its effects on mechanical properties:

By varying the parameters such as growth rate(R) and temperature gradient(G_L) one can exercise control over the microstructure of the directionally solidified alloys. This control on microstructure could lead to the control of mechanical properties. In this section we will see how solidification parameters control the mechanical properties of

directionally solidified alloys.

(2.3.1) Effect of interlamellar or rod spacing on mechanical properties:

It is well known that increase in growth rate leads to decrease in interlamellar or interrod spacing. In other words increase in R would bring finer microstructure to the in-situ composites. The finer microstructure in in-situ composites can give rise to a considerable strengthening effect that is not predicted by the rule of mixtures. Davidson et al.[26] have studied the effect of interlamellar spacing on the yield strength of $Al-CuAl_2$ eutectic composites. Their results predict that the yield stress decreases with the increase in lamellar spacing as shown in Fig 2.11. The result has been successfully explained by the modified Hall-Petch relation;

$$\sigma_c = \sigma_0 + k \lambda^{-0.5}$$ (2.8)

where; σ_c = composite yield stress and

               λ = interlamellar spacing.

It is claimed that dislocations generated in the weaker aluminum phase pile-up at the lamellar interfaces as the interface is incoherent although no microstructural evidence has been provided for this claim. And since there are more lamellae per unit volume when the growth rate is high there will be several such dislocation pile-ups leading to increase in yield strength. But this explanation has been modified by Shaw [27] after observing the Cd-Zn lamellar composite. Though the lamellar interface is coherent (Lattice parameter 'a' of the two phases present in Cd-Zn system differ
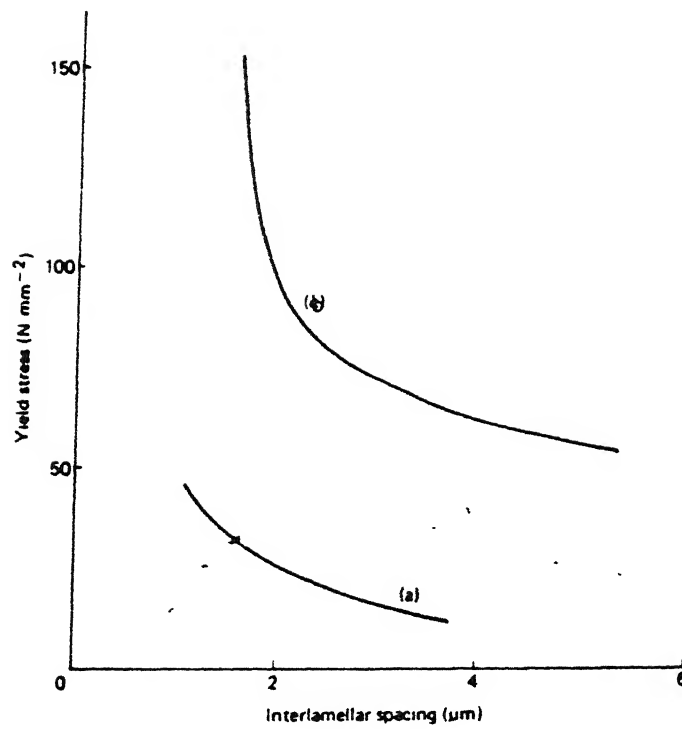
Fig.2.11 The variation of yield stress with interlamellar spacing of an Al-CuAl$_2$ eutectic composite. (a) Annealed at 300°C, (b) Transverse direction.
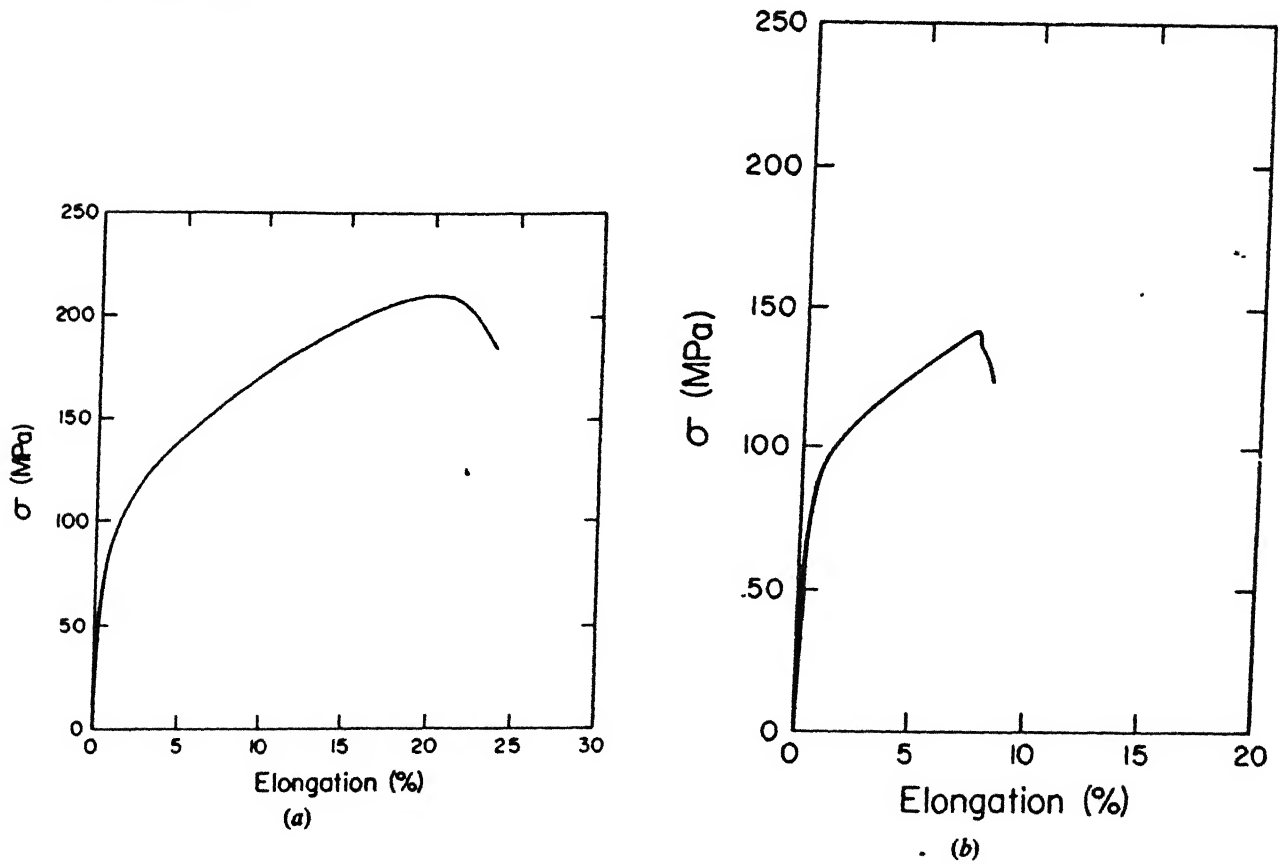
Fig.2.12 Typical stress-strain curves for Al-4wt% Cu columnar alloys, (a) Longitudinal direction, (b) Transverse direction.

only by 10%) a similar relationship as in Al-CuAl$_2$ of σ_c vs λ was observed by Shaw. This result shows that the yield strength of the alloy is not just because of in coherent interface. A more likely source of interference to dislocation movement is the increasing density of grown-in defects as the growth velocity increases. The variation of rupture stress, σ_r, with change in λ for Ni-Sn eutectic system has been experimentally found by Dirnfled et al.[28]. There is marked increase in strength with decreasing interlamellar spacing. The tensile rupture stress, σ_r, is 5.3 Kgf mm^{-2} at λ = 13.5 μm (R = 1mm/h) and 11.5 Kgf mm^{-2} at λ = 8.3μm (R = 10mm/h).

(2.3.2) Effect of growth velocity on mechanical properties:

Cantor et al. [29] have examined the influence of sudden changes in growth velocity on the structure of Al-Al$_3$Ni composite. They found that such changes lead to the breakdown of planar to cellular eutectic coupled growth (This may be due to the presence of small amount of impurities or small deviation from eutectic composition) or a change in the grain size. These growth irregularities change the properties of the composite as it is evident in Al-Al$_3$Ni case. The cellular eutectic Al-Al$_3$Ni composites exhibit a reduced room temperature ultimate tensile strength (UTS) of 220 Nmm^{-2} compared to 297Nmm^{-2} for the fully directional composites. At the same time increase in ductility has been observed. Sudden increase in growth velocity could lead to misaligned fibers of Al$_3$Ni, which do not provide reinforcement and result in a reduced UTS.

(2.3.3) Anisotropy in mechanical properties of directionally solidified alloys:

An important property of directionally solidified samples is anisotropy in mechanical properties. An investigation in this direction has been done by Hiroshikato [30]. He has observed the anisotropy in tensile properties in Al-4 wt% Cu alloys. The typical tensile curves of longitudinal and transverse specimens are shown in Figs 2.12(a) and 2.12(b).

(2.3.4) Growth parameters and their effect on creep properties of in-situ composites:

The high temperature stability, large aspect ratio (ratio of the largest to the smallest dimension of a phase) and strong interface bonding found in many in-situ composites contribute to their good creep resistance. The solidification parameters such as G_L and R have been found to effect the various creep properties such as rupture life and minimum creep rate. Mc Lean et al. [31] have studied the creep behaviour of Ni, $Ni_3Al-Cr_3C_2$ composites with respect to the solidification parameters. The results of their studies are shown in Figs 2.13(a) and 2.13(b). Figures 2.13(a) and 2.13(b) show that the rupture life increases and the minimum creep rate decreases as the interfibre spacing decreases. It is also clear from the figure that rupture life decreases after certain rate of solidification. The enhancement of creep properties persists only as long as the eutectic interface remains planar. The deterioration in properties coincide with the onset of cellular eutectic growth at higher rate of freezing. Enhancement of properties with reduction in spacing occurs in several other composites.

In another study done by Versnyder et
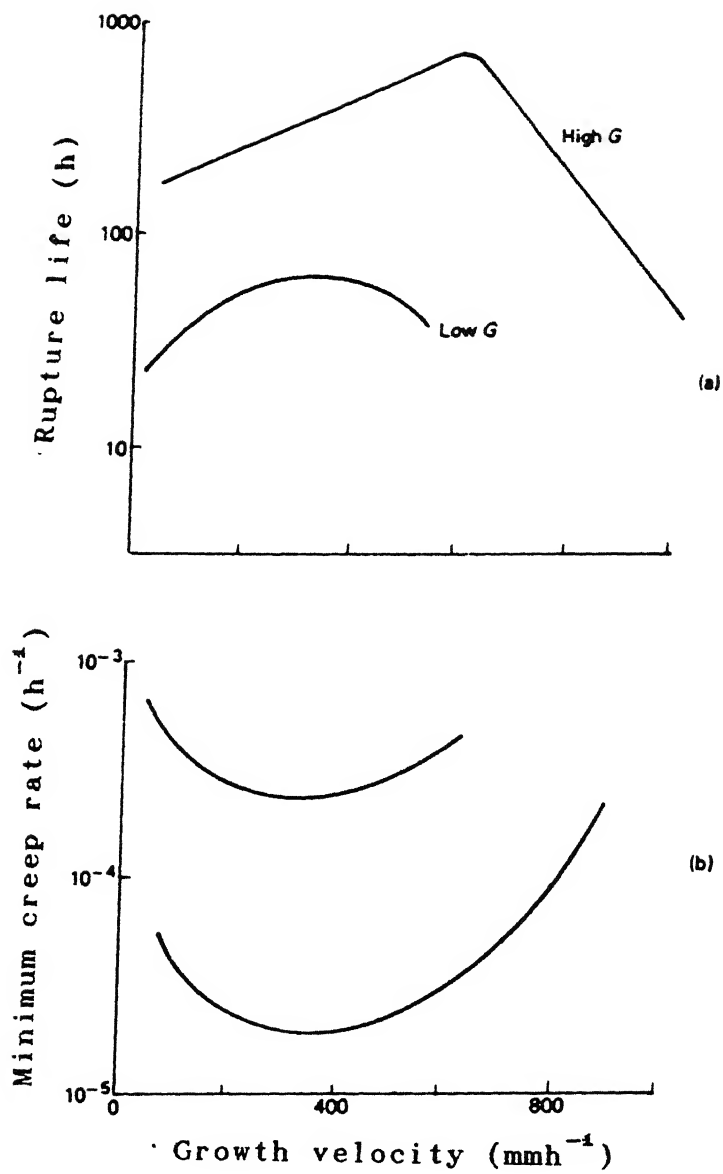
Fig.2.13 Creep behaviour of Ni, $Ni_3Al- Cr_3C_2$ composite tested at $980^{\circ}C$ and $122\ Nm^{-2}$,(a) Log(rupture life) as a function of growth velocity, (b) Log(minimum creep rate) as a function of growth velocity.

al.[32] have found significant changes in creep behaviour of Mar-M200 alloys depending on the nature of solidification. The result of their experiment for conventionally cast (C), directionally solidified (D) and monocrystals (M) are shown in Fig 2.14.

The better properties of the columnar and monocrystal material result from a number of factors. They are,(a)Improved distribution of inclusions,(b)Reduced microporosity, (c) The alignment of as-cast grain boundaries with direction of stress, (d) The preferred crystalographic texture of the columnar material also has an effect. (e)The distribution of microsegregation in the columnar material is more uniform than that of the conventionally cast material which also could enhance the mechanical properties.

(2.3.5) Effect of directional solidification on resistance to hydrogen embrittlement:

A very important observation of effect of directional solidification on Hydrogen embrittlement has been carried out by Liu and Li et al.[33]. They have compared the Hydrogen embrittlement effect on wrought conventionally cast and directionally solidified stainless steels. The results of their observations proved that directionally solidified steel offers better resistance to Hydrogen embrittlement than others. The Hydrogen embrittlement takes place because of accumulation of Hydrogen at the Austenite - Ferrite phase boundaries. The ferrite columns grow directionally right across whole sample in the directionally solidified samples, on the contrary in conventionally cast samples, Ferrite is distributed in an
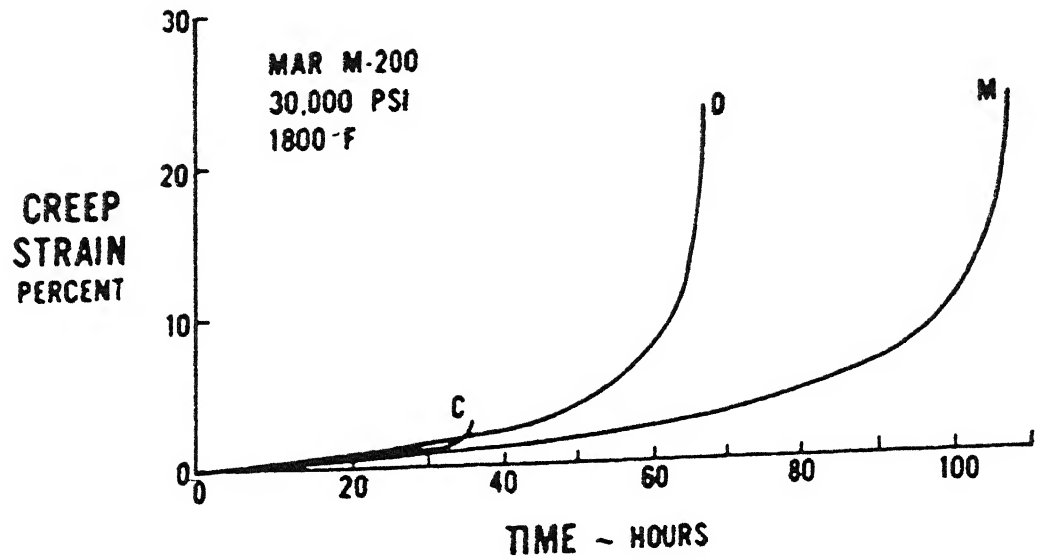
Fig2.14 Comparison of the creep properties at $1800^{\circ}F$ of conventional(C), directional(D), and monocrystal(M) Mar-M200.

isolated manner. It is certain that Hydrogen is accumulated at the Austenite - Ferrite phase boundary because Hydrogen solubility in Austenite is greater than that in Ferrite and Hydrogen diffusivity in Ferrite is much greater than that in Austenite. In steel with isolated Ferrite, hydrogen accumulation cannot be decreased, this is the site of easy crack initiation and premature failure. As a result resistance to Hydrogen embrittlement is lowered. In the directionally solidified samples, however, Hydrogen is also enriched at the Austenite - Ferrite phase boundary but the Hydrogen can diffuse out along the aligned Ferrite phase boundary, and resistance to Hydrogen embrittlement of the directionally solidified sample is better than that of conventionally cast samples in which ferrite is isolatedly distributed.

(2.3.6) Fibre coarsening of in-situ composites:

Intrinsically, in-situ composites are very stable at high temperatures. This characteristic is derived from their solidification under near-equilibrium conditions coupled with the formation of low energy boundaries. However, acceptable performance depends on long term microstructural stability at elevated temperatures in order to maintain the integrity of mechanical properties. The main reasons for degradation of properties of in-situ composites could be oxidation, matrix - fibre interaction and shape and size instabilities. It has been observed that in some systems shape and size variations of the fibres lead to coarsening of fibers and hence deterioration of properties. Fibre coarsening has been examined most extensively in the $Al-Al_3Ni$ [34,35] system. Figs

2.15(a) & 2.15(b) show some selective kinetic measurements of coarsening of Al-Al$_3$Ni system. It is clear from the figure that fibre density (number of fibres per unit volume) decreases with increase in time of exposure of the composite to high temperature environment. And since fibre density is inversely related to coarsening it means that coarsening is taking place. Several theories have been proposed to explain the coarsening. One of them is Ostwald coarsening or ripening [36]. According to this theory coarsening occurs because of dissimilarity in the fibre radii of the composite. Fibres of large radii grow at the expense of smaller radii fibres because this process leads to decrease in free energy of the system. According to this theory fibre density is related to coarsening time;

$$\rho^{-3/2} - \rho_0^{-3/2} = K.Exp-\left[\frac{Q_D + Q_S}{RT}\right](t-t_0) \qquad (2.9)$$

Where,

ρ_0-is initial fibre density,

k -is a constant,

Q_D-is activation energy for diffusion,

Q_S-is heat of solution and

t_0-is incubation time for finite size fibres to commence dissolving.

This theory predicts the incubation time (t_0) for a coarsening process to commence. It has been found that the t_0 value depends on various factors such as temperature of exposure and growth morphology. Carefully grown composites can show a relatively fault free structure of fibres of uniform diameter and a large t_0 value is expected in such a
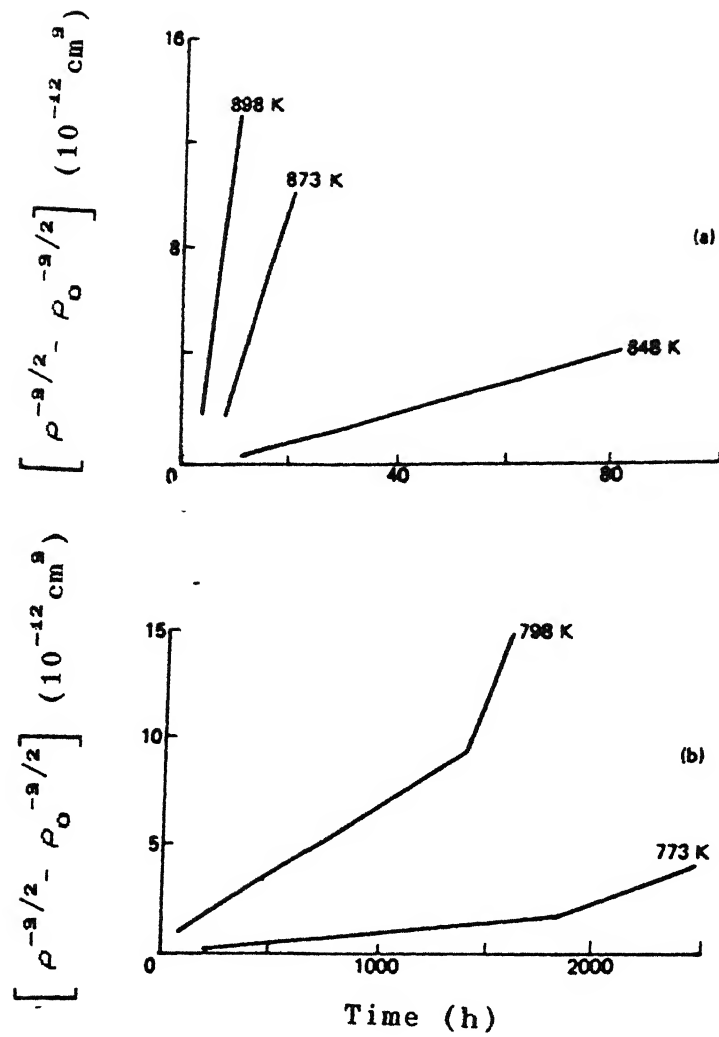
Fig.2.15 (Fibre density)$^{-3/2}$ as a function of coarsening time for the Al- Al$_3$Ni composite.

composite.

(2.4) Electromagnetic properties of eutectic in-situ composites:

Eutectic in-situ composites have potential applications in the field of magnetic materials. Several investigations show that some of the directionally solidified eutectics can be used as permanent magnetic materials. A permanent magnetic material must have a very high internal coercive force. If one wants a ferromagnetic substance with a high internal coercive force, one has to impede the domain boundary movement when the applied field is reversed. As in the case of permanent magnet steels , this may be achieved by introducing non magnetic inclusions, lattice defects, internal strains or inhomogeneities in to the material. Higher values of the coercive force can be obtained if the magnet is composed of such small particles that, form energy considerations, only a single domain can be formed in it. The coercive force may then be determined by the crystal anisotropy as for Alnico or Barium Ferrite. An interesting alternative approach to the problem of finding high coercive force particles was suggested by the shape anisotropy effect [37]. If the diameter of an elongated ferromagnetic particle decreased below a critical value, under magnetisation reversal, the spins must rotate in union. As a result, a rod like particle of isotropic material exhibits a strong magnetic anisotropy, in addition to the coercive force parallel to the axis increases to a maximum value equal to half the saturation magnetisation.The critical diameter is of the order of 100 Angstroms. Therefore, if one is able to align very thin ferromagnetic rods parallel to one another, one gets a

substance with a high coercive force. Directionally solidified InSb - MnSb eutectic has a MnSb ferromagnetic phase with a volume ratio of 6.9% consists of parallel aligned, needle-shaped particles in a non magnetic matrix. If the rate of solidification is around 2Cm/h the diameter of the rod is between 1 & 2μm. This diameter is not small enough to prevent domain wall movement. However, in principle there exists the possibility of reducing the cross section of the ferromagnetic needle-shaped inclusions by increasing the growth rate and wire-drawing afterwards. In the InSb - NiSb system for instance the diameter of the needle decreases from 5.0 to 0.5μm if the growth rate is increased from 0.01mm/minute to 1mm/minute [38]. A similar result was obtained by Livingston in the Au - Co eutectic. The diameter of the Cobalt needles decreased with increasing growth rate, the coercive force increased by an order of magnitude. At a rate of 2.1mm/sec the coercive force reached 330 Oe. The coercive force increased substantially when the rod diameter was reduced by wire drawing, value of 925 Oe was obtained. In the case of unaligned solidification of the same system, the coercive force was small and isotropic.

These experiments demonstrate that the intrinsic coercive force increases with the increasing growth rate. However, the usefulness of the method of increasing growth rate is limited, since at higher rates the microstructure is more lamellar than rod - like. This again reduces the coercive force. In the above mentioned eutectics the matrices are non - magnetic. This has the disadvantage that the attainable energy products are limited by the volume fraction of the ferro

magnetic phase.

Small dimensions of the order of 100 Angstroms are also necessary for the dispersed phase in superconducting eutectics. Because the critical magnetic field increases on decreasing the thickness of the thin wires or lamellae of superconducting material.

The InSb - NiSb eutectic composite has a very useful magnetoresistance effect. The InSb matrix is semiconducting and the NiSb fibres are conducting. If the fibres and applied electric and magnetic fields are mutually perpendicular the NiSb fibres short circuit the InSb Hall voltage and allow the electrons in the InSb to respond to the Lorentz force and flow at an angle to the applied electric field. This Hall angle increases as the magnetic field increases and the increasing length of the current path produces a large increase in the systems. This method of varying resistance has been used in a variety of devices including field sensors, current transducers and contactless potentiometers.

An investigation into the magnetic properties of Bi - Mn eutectic alloys [39] shows that the directionally solidified samples have a non-magnetic Bi phase dispersed with Bi - Mn ferromagnetic needles. The alloys show magnetic anisotropy in a direction of solidification and that the intrinsic coercivity is maximum in the direction of solidification. The following table (table 2.1 briefly explains the application of eutectics in the field of electromagnetism.

The main difficulty with regard to the practical applications of eutectics is that of finding the best

Table 2.1 Electromagnetic properties of eutectic composites.

Matrix Inclusion	Metal	Semiconductor	Insulator
Metal	Magnetism, Super Conductivity.	Galvano magnatic, Thermal, Optical.	Optical.
Semiconductor	-	-	-
Insulator	-	-	Optical

possible system. Moreover the limited volume fraction of the second phase has become the main constraint for their applications.

EXPERIMENTAL METHODS

(3.1) Preparation of a master alloy:

Al and Ni of 99.99% purity have been used to prepare Al-Ni master alloy of 33.5 wt% Ni. The melting is carried out at about $1400^{o}C$ using a graphite crucible of 1 inch internal diameter and 1.5 inch long in an induction furnace (AJAX induction furnace, 20000 Hz). The crucible was surrounded by a graphite susceptor which inturn was enclosed in a refractory sheath of about 0.5 inch thickness. The whole assembly was enclosed in a 4 inch diameter quartz tubing. The sheath was to insulate the quartz tubing against the heated susceptor. Before starting the induction furnace the quartz tubing was evacuated to a pressure of 10^{-5} atmosphere and flushed with high purity argon gas thrice. The composition of the master alloy as determined by gravimetric analysis is found to be 34.75 wt% Ni. The reagent used for chemical analysis is Dimethyl Glyoxime-DMG.

(3.2) Preparation of the eutectic alloy:

Preparation of the eutectic alloy is also done by using the same induction melting furnace as above in graphite crucibles.The master alloy after filing off the outer oxidised layer was diluted sufficiently with Al to produce a number of Al-5.7wt% Ni eutectic alloy ingots of 1 inch diameter and 1.5 inch long.Composition analysis of the alloy is done by using a microprobe(Jeol Scanning electron microscope-JSM-840.A).All the alloy ingots are found to have a composition of 5.9wt% Ni. For each compositional analysis an area of 50x75 square microns is considered. The two areas

considered for analysis are approximately 0.5 and 1.2 inch

distance from the bottom of the 1.5 inch long alloy ingot. The

polished surface of the eutectic as cast alloy was etched with

Kellers reagent (2.5 ml H_2SO_4, 1.5 ml HNO_3, 1.0 ml HF and 95 ml

H_2O) for observing the microstructure

(3.3) Directional solidification:

(3.3.a) Experimental set-up:

Schematic diagram of the experimental

set-up is shown in Fig 3.1. A small resistance furnace of 20cm

length mounted on a vertical phase is used. A Vycor tube of

approximately 2 inch diameter with upper end tapered to

approximate 1cm diameter is inserted into the furnace as shown

in figure. The lower end of the Vycor tube is connected to an

Argon gas supply cylinder through a gas bubler and a tube

containing calcium chloride($CaCl_2$). Calcium chloride is used to

absorb moisture in the Argon gas. The eutectic alloy is taken in

a graphite crucible attached to a copper chill at the bottom.

The chill and the crucible assembly is held in position inside

the top end of the furnace by a refractory wire wound on to the

shaft of a small drive motor through a pulley. In actual

experiment, the crucible-chill assembly is externally lowered

into the furnace at a constant speed. The schematic diagrams of

the crucible and copper chill especially prepared for our

requirements are shown in Figs 3.2(a) and 3.2(b).

Temperature profile of the furnace

along it's axis is determined by using a Chromel-Alumel

thermocouple connected to a digital millivoltmeter. The

temperature profile and corresponding values are shown in Fig

3.3 &table 3.1respectively. The average speed provided by the
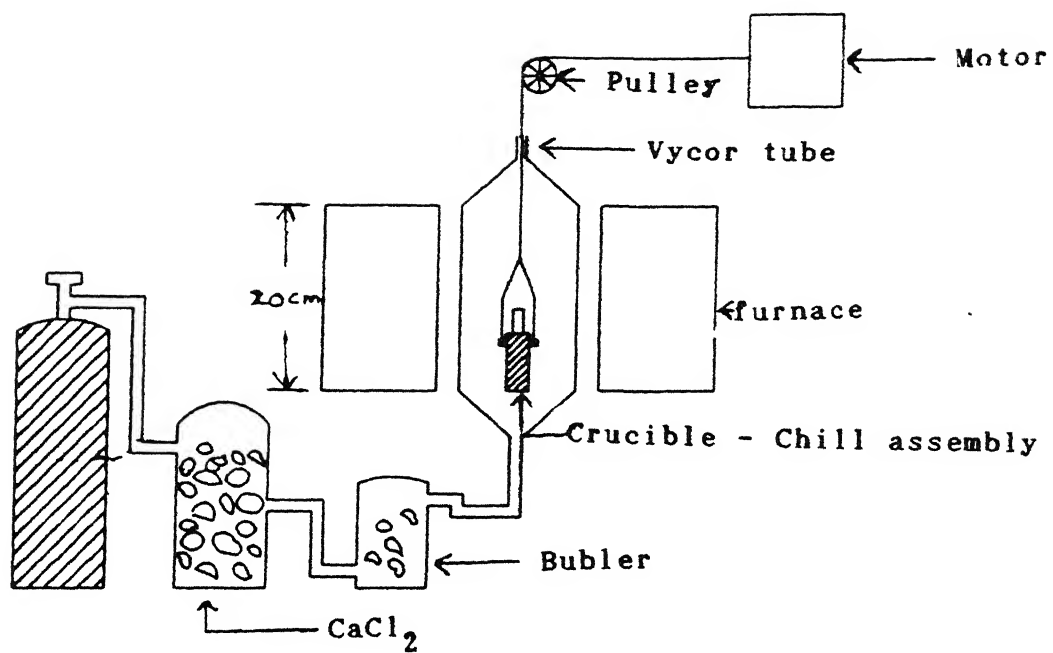
Fig.3.1 Schematic diagram of the experimental set-up.
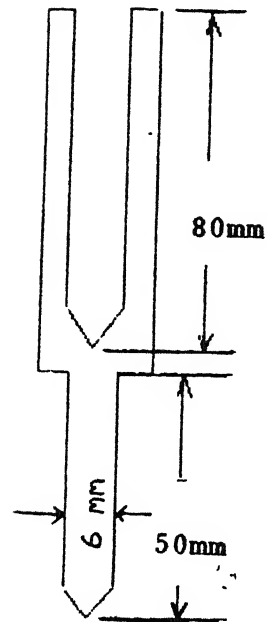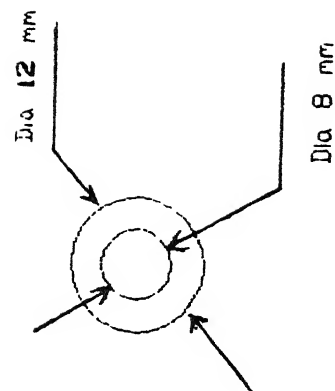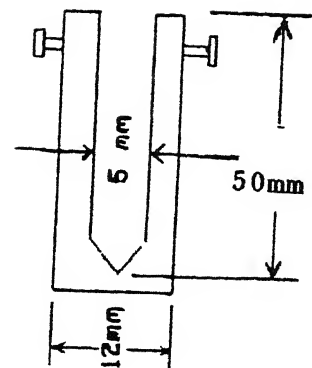
Fig.3.2 (a) Crucible, (b) Chill,
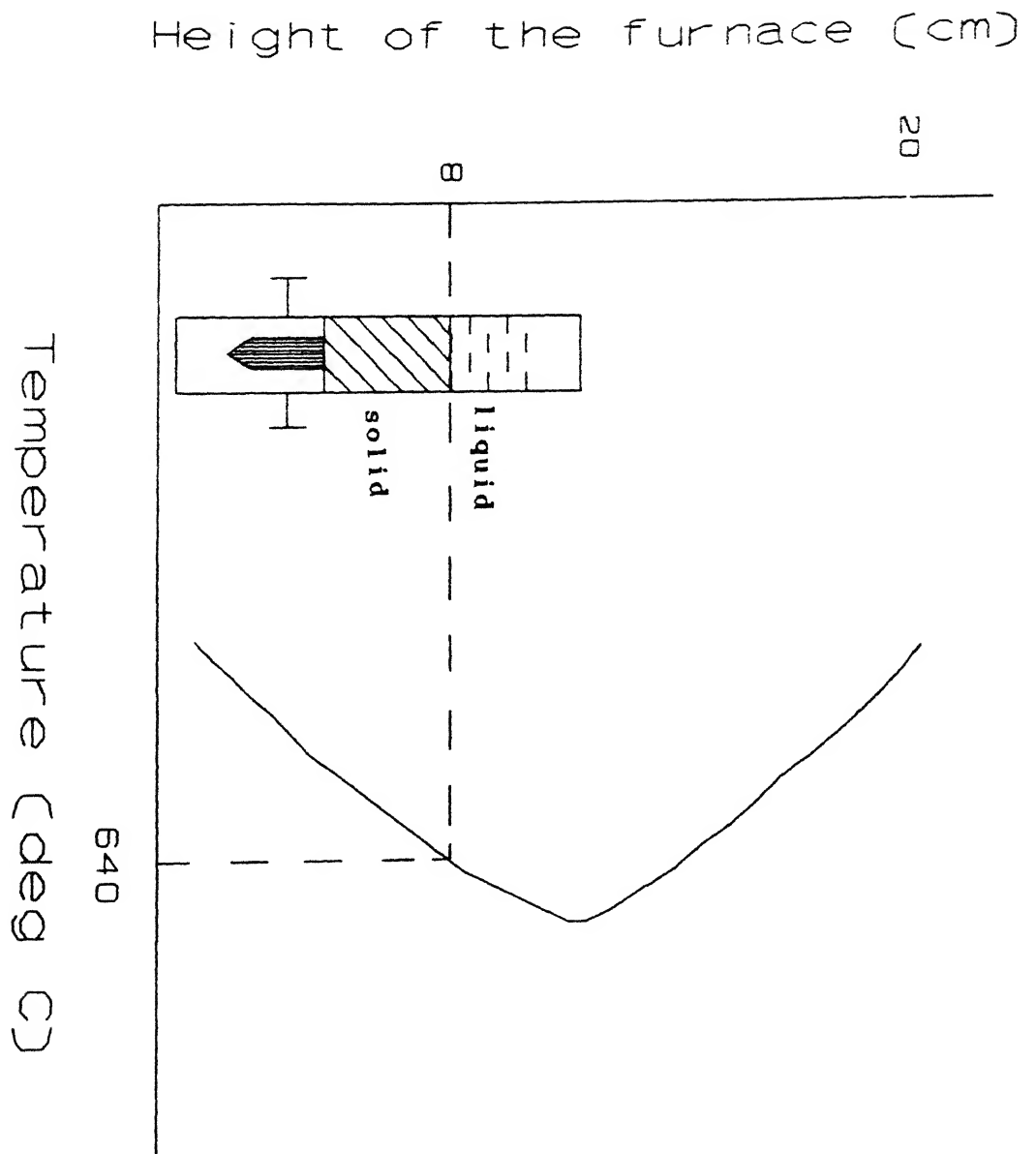
Fig. 3.3 Temperature variation along the axis of the furnace as a function of height.

Table 3.1 Temperature variation along the axis of the furnace as a function of height.

Distance from the bottom of the furnace (cm)	Digital Voltmeter Reading (mV)	Temperature ($^{\circ}$C)
2.0	18.3	445
4.0	23.5	568
6.0	24.8	598
8.0	26.9	648
10.0	27.8	668
12.0	29.8	716
14.0	29.3	704
16.0	28.0	675
18.0	25.0	603

Table 3.2 Speed of the motor.

Distance moved by the crucible	Time (sec)	Speed (μm/sec)
1.0	1316	7.60
2.0	2484	8.05
3.0	3720	8.06
Average Speed		7.90

drive motor for lowering the crucible-chill assembly found to be 7.9 $\times$ 10^{-4} cm/sec which is shown in table 3.2.

(3.3.b) Experiment:

The eutectic alloy prepared earlier is swaged to fit into the graphite crucible of inner diameter 8mm. After inserting the swaged piece into the crucible,the crucible-chill assembly is lowered into the vycor tube as shown in Fig 3.1. DS is carried out at a rate of 7.9 $\times$ 10^{-4} cm/sec under Argon atmosphere with the temperature gradient(G_L) maintained at 25°C/Cm. For the purpose of solute distribution analysis and to freez the events at the S-L interface the eutectic alloy is partially directionally solidified in another run under the identical conditions as before to a length of about 4.5Cm and then instantaneously quenched by dropping the entire crucible-chill assembly in liquid Nitrogen in about 0.28sec (this is the time of flight for the charge to reach the LN_2 bath from the furnace position). After polishing the quenched ingot,the length of the quenched section was found to be about 2.5Cm. A 2 Cm long section of the ingot is cut to provide equal lengths of the DS and frozen sections. A longitudinal section on this piece is polished to expose a planar section for different microstructural observations and measurements.The microstructural observations are carried out by etching the ingot with Kellers reagent.

(3.4) Hardness measurements:

Vickers microhardness measurements are taken using Leitz Miniload2 instrument along the longitudinal direction of the ingot containing the frozen in interface to examine the variation of hardness in the directionally

solidified and quenched sections. A 1.5mm interval is chosen for the hardness measurements.

(3.5) X-Ray and microprobe analysis:

Laue back reflection pinhole patterns are taken using ISO-DEBYFLEX 2002 at different sections of the ingot to ascertain the crystallinity of the material. After confirming the fact that grain size in quenched section is larger than the X-ray beam diameter from pin hole pattern the quenched ingot is polished using chemical polish (a mixture of HNO_3, H_3PO_4 AND CH_3COOH) and later etched with Kellers reagent to find the grain size of the quenched section. Microprobe analysis is done around a selected β-phase(Al_3Ni) rod using JSM-840.A instrument to determine the solute distribution. The analysis is done both in longitudinal and transverse directions using polished section of the ingot containing the frozen in interface. In the longitudinal direction, analysis is done on the Al_3Ni rod and on neighbouring matrix through the interface into the quenched section. Spot analysis(500 Angstroms) is used to ascertain the stoichiometry of the actual phases and area analysis to determine the solute distribution. Each point on a profile into the quenched section is obtained by analysing an area of 50 X 75 square microns where as in the DS section it is done both by spot and area analysis. similarly the analysis in the transverse direction is done at a 3 microns distance ahead of the interface into the quenched side of the ingot.

(3.6) Problems in alloy making:

Aluminum crucibles used in induction melting are found to fail repeatedly with the aluminum alloy melt.Successive melting of all alloys however was finally done

in graphite crucible. Directional solidification of these alloys in other than graphite was found to give raise to serious contamination problems, for example solidification in stainless steel tubes was jinxed right from the beginning with very deleterious contamination of the element of the stainless steel tube, which gave riser to the formation of extraneous phases directly interfering in the alignment of Al_3Ni rods during directional solidification.

CHAPTER 4

THEORETICAL ANALYSIS OF THE SOLUTE DISTRIBUTION

Theoretical analysis of the solute distribution around a growing β - phase is done in this chapter. For doing this analysis S-L interface is assumed to be planar. With this assumption and with the aid of appropriate boundary conditions solutions of the diffusion equation can be obtained.

Solution of the diffusion equation:

We take the planar S-L interface to be uniformly moving with a velocity R as shown in Figure 4.1 and containing a distribution of the β precipitates growing progressively with the motion of S-L interface and aligned normally to the advancing interface.

Under conditions of DS, if the interface is made to move at a steady rate R through an externally fixed temperature gradient (G_L), with constant heat extraction from the solidified ingot, the overall characteristics will then be determined by the rate of advance of the interface and the solute diffusion fields from the liquid to the S-L interface. The time dependent diffusion equation is,

$$\nabla^2 C_L = \frac{1}{D_L} \cdot \frac{\partial C_L}{\partial t} \qquad (4.1)$$

where ∇^2 is the usual Laplacian operator in rectangular co-ordinates, C_L is solute concentration in the liquid, D_L is the solute diffusivity in the liquid and t is the time. We choose as shown in Fig.4.1, the origin of the co-ordinates at the centre of the growing tip of a β precipitate particle with
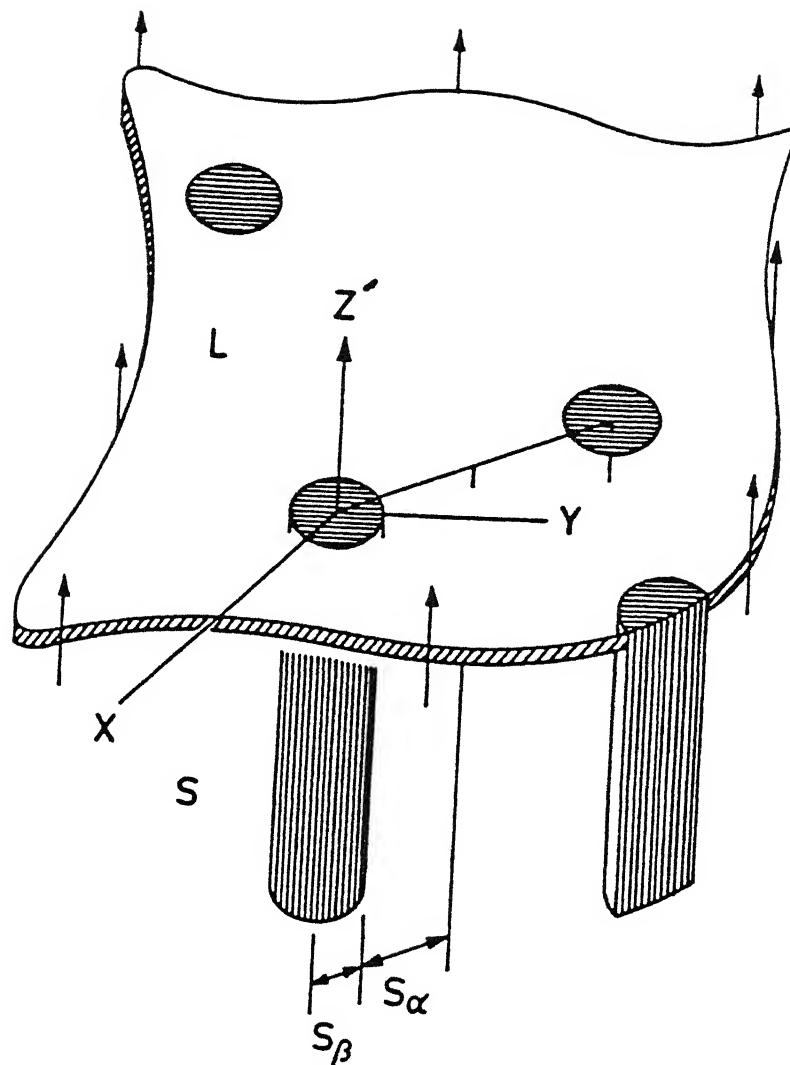
Fig 4.1 Advancing solid - liquid interface with the coordinates marked.

the Z-axis taken parallel to its cylindrical axis. If the interface is moving at a steady rate R along the Z-axis, then we may take $Z' = Z - Rt$ as the moving co-ordinate and the equation (4.1) becomes;

$$\frac{\partial^2 C_L}{\partial X^2} + \frac{\partial^2 C_L}{\partial Y^2} + \frac{\partial^2 C_L}{\partial Z'^2} = -\frac{R}{D_L} \cdot \frac{\partial C_L}{\partial Z'} \qquad (4.2)$$

In cylindrical co-ordinates r, θ, Z' ignoring angular dependence of concentration,

$$\frac{\partial^2 C_L}{\partial r^2} + \frac{1}{r} \cdot \frac{\partial C_L}{\partial r} + \frac{\partial^2 C_L}{\partial Z'^2} \quad \frac{R}{D_L} \cdot \frac{\partial C_L}{\partial Z'} = 0 \qquad (4.3)$$

choosing dimensionless variables, $\qquad r^* = \delta r = \dfrac{r}{S_\alpha + S_\beta}$,

$$S_\beta^* = \delta S_\beta = \frac{S_\beta}{S_\alpha + S_\beta} \quad , \quad Z'^* = \delta Z' = \frac{Z'}{S_\alpha + S_\beta} \quad \text{and}$$

$a = \dfrac{R(S_\alpha + S_\beta)}{D_L}$ with $S_\alpha + S_\beta$ as our unit of measure equation (4.3) becomes,

$$\frac{\partial^2 C_L}{\partial r^{*2}} + \frac{1}{r^*} \cdot \frac{\partial C_L}{\partial r^*} + \frac{\partial^2 C_L}{\partial Z^{*2}} + a \cdot \frac{\partial C_L}{\partial Z'} = 0 \qquad (4.4)$$

choosing a product solution,

$$C_L = C_L (r^*) \cdot C_L (Z^*) \qquad (4.5)$$

and substituting (4.5) in (4.4) leads to,

$$\frac{d^2 C_L (Z^*)}{dZ^{*2}} + a \cdot \frac{d C_L (Z^*)}{dZ^*} - K_1^2 \cdot C_L (Z^*) = 0 \qquad (4.6)$$

$$\frac{d^2 C_L (r^*)}{dr^{*2}} + \frac{1}{r^*} \cdot \frac{d C_L (r^*)}{dr^*} + K_1^2 \cdot C_L (r^*) = 0 \qquad (4.7)$$

where K_1 is the dimensionless separation constant. The particular solutions of the equations are,

$$C_L(\delta r, \delta z') = Exp\left[-\frac{a}{2}\left\{1 \pm \sqrt{1 + \frac{4Kl^2}{a^2}}\right\}\delta z'\right]J_0(K_L\delta r) \quad (4.8)$$

where, J_0 is the Bessel function of the first kind. General solution obtained as a linear combination of particular solutions in terms of the dimensionless co-ordinates is

$$C_L(r,Z') = \sum_{l=1}^{\infty} A_l Exp\left[-\frac{a}{2}\left\{1 \pm \sqrt{1 + \frac{4Kl^2}{a^2}}\right\}\delta z'\right]J_0(K_L\delta r) \quad (4.9)$$

where, the linar coefficients A_l and the eigenvalues K_l are to be determined from the boundary conditions. Here, all the boundary conditions given by Flemings for lamellar eutectics with suitable modifications are used.

Boundry conditions

(1) $C_L(r,z')\Big|_{z'=\infty} = C_E$, the eutetic composition,

(2) $\dfrac{\partial C_L}{\partial r}\Big|_{r=0} = 0$

(3) $\dfrac{\partial C_L}{\partial r}\Big|_{r=S_\alpha + S_\beta} = 0$

(4) $-\dfrac{\partial C_L}{\partial z'}\Big|_{z'=0} = \dfrac{R}{D_L}\cdot(C_E - C_{\alpha M})$, $S_\beta \leq r \leq S_\alpha + S_\beta$

(5) $-\dfrac{\partial C_L}{\partial z'}\Big| = -\dfrac{R}{D_L}\cdot(C_E - C_{\beta M})$, $0 \leq r \leq S_\beta$

where, $C_{\alpha M}$ and $C_{\beta M}$ are respectively the solute concentrations of α and β phases. In the present system $C_E = 5.9$ Wt% Ni, $C_{\alpha M} = 0.05$ Wt% Ni and $C_{\beta M} = 42.05$ Wt% Ni corresponding to the intermetallic AlNi. From the appendix, the complete solution satisfying the above set of boundary conditions is;

$$C_L = C_E - \sum_{l=1}^{\infty} A_l \, \mathrm{Exp}\left[-\frac{a}{2}\left\{ 1 + \sqrt{1 + \frac{4Kl^2}{a^2}} \right\}\delta Z \cdot \right] J_0(K_L \delta r) \qquad (4.10)$$

Where,

$$A_l = \frac{4\left[C_{\beta M} - C_{\alpha M} \right]}{\left\{ 1 + \sqrt{1 + \frac{4Kl^2}{a^2}} \right\}} \cdot \frac{J_1(K_1 \cdot \delta S_\beta)}{K_1\left[J_0(K_1) \right]} \qquad (4.11)$$

The eigen values K_1 are determined by the roots of $J_1(K_1) = 0$ and for the purpose of discussion the above equation (4.10) is written as;

$$C_L = C_E - \sum \qquad (4.12)$$

CHAPTER 5

RESULTS AND DISCUSSION

(5.1) Microstructures:

The microstructures of the as-cast, directionally solidified (both longitudinal and transverse sections) and the quenched interface are shown in Figs. 5.1, 5.2, 5.3, 5.4 respectively. Line analysis on directionally solidified section for both Al and Ni are shown in Figs. 5.5. The phase diagram of Al-Ni system is shown in Fig. 5.6.

The comparison of the micrographs of the as-cast and directionally solidified clearly shows that directional solidification of the eutectic has lead to the formation of aligned rods of the Al_3Ni phase. The average interrod spacing $\lambda = 2 (S_\alpha + S_\beta)$ is found to be 14.5 microns at the growth rate of R = 7.9 x 10^{-4} cm/sec and temperature gradient G_L of 298K/cm.

The line analysis shows that the β rods have higher concentration of Ni than the matrix which is expected. The observation of the interface structure reveals that there are two solidification fronts one ahead of the other. The leading eutectic front is found to be in the peripheries of the ingot whereas the lagging front is at the center of the ingot. The reason for the formation of two fronts instead of a single one could be the variation in local temperature gradient and hence growth velocities.

(5.2) The inter rod spacing λ = 14.5 microns found from the experiment fit very well on an extended plot of the inter rod spacing versus growth rate obtained by Livingston et al. for the same system. The plot with the experimental point is shown in Fig.5.6. Similar measurements from an earlier thesis are also
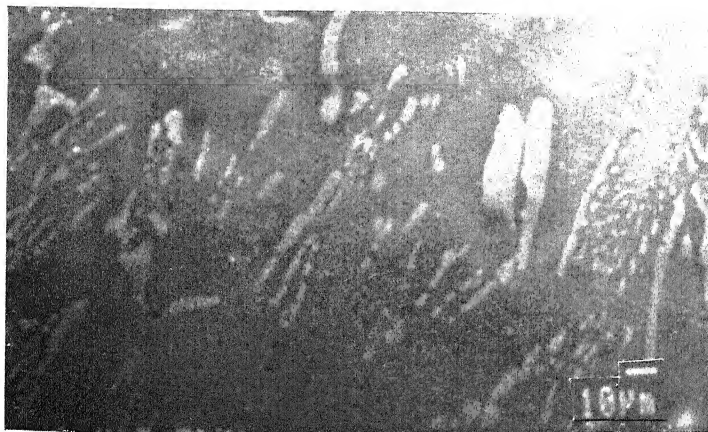
Fig 5.1 Microstructure of the as cast Al – 5.7 wt% Ni eutectic alloy.
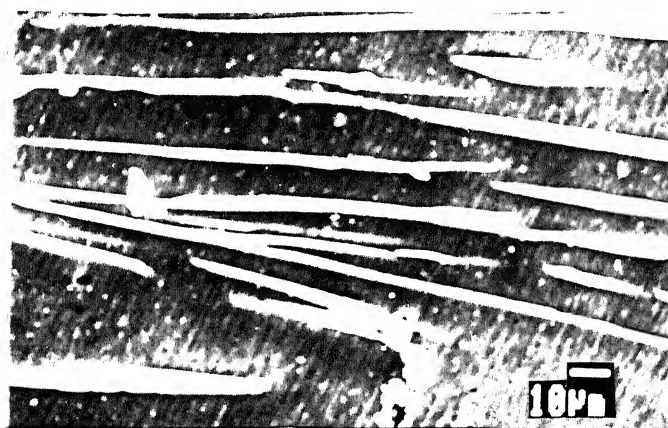
Fig 5.2 Microstructure of the directionally solidified Al – Ni eutecticalloy (longitudinal)
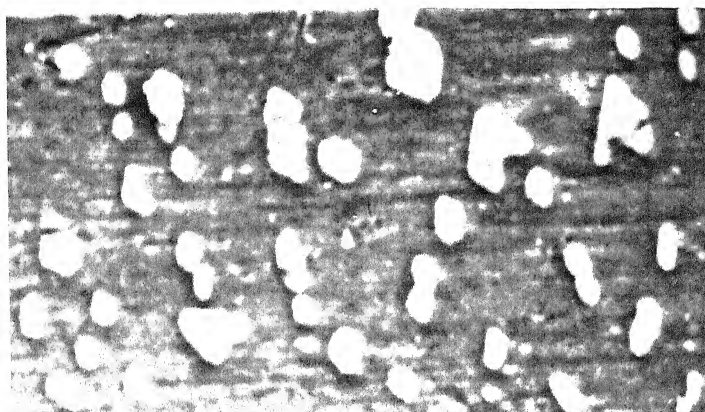
Fig 5.3 Microstructure of the directionally solidified
Al - 5.7 wt% Ni eutectic alloy (transverse)
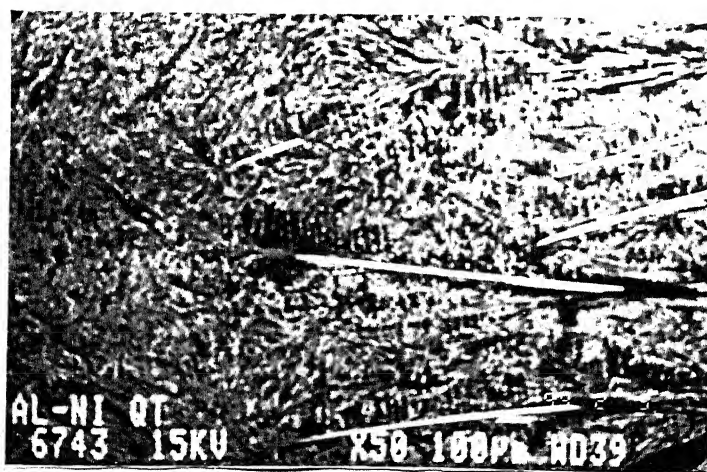
Fig 5.4 Microstructure of the quenched interface of Al
- Ni eutectic alloy.
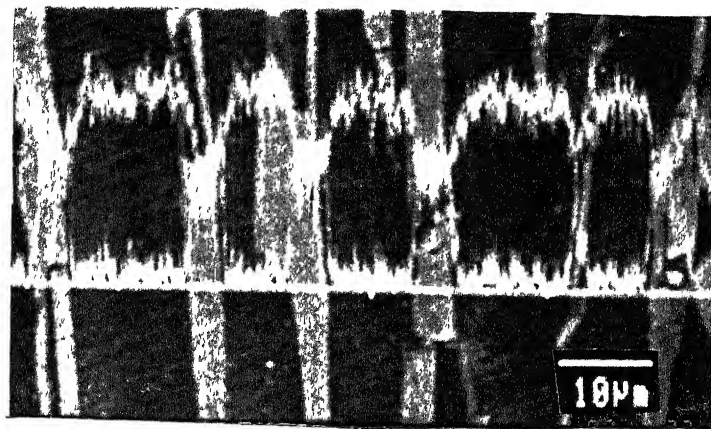
Fig 5.5 Microstructure of the directionally solidified Al – Ni eutectic alloy showing the line analysis for both Al and Ni.
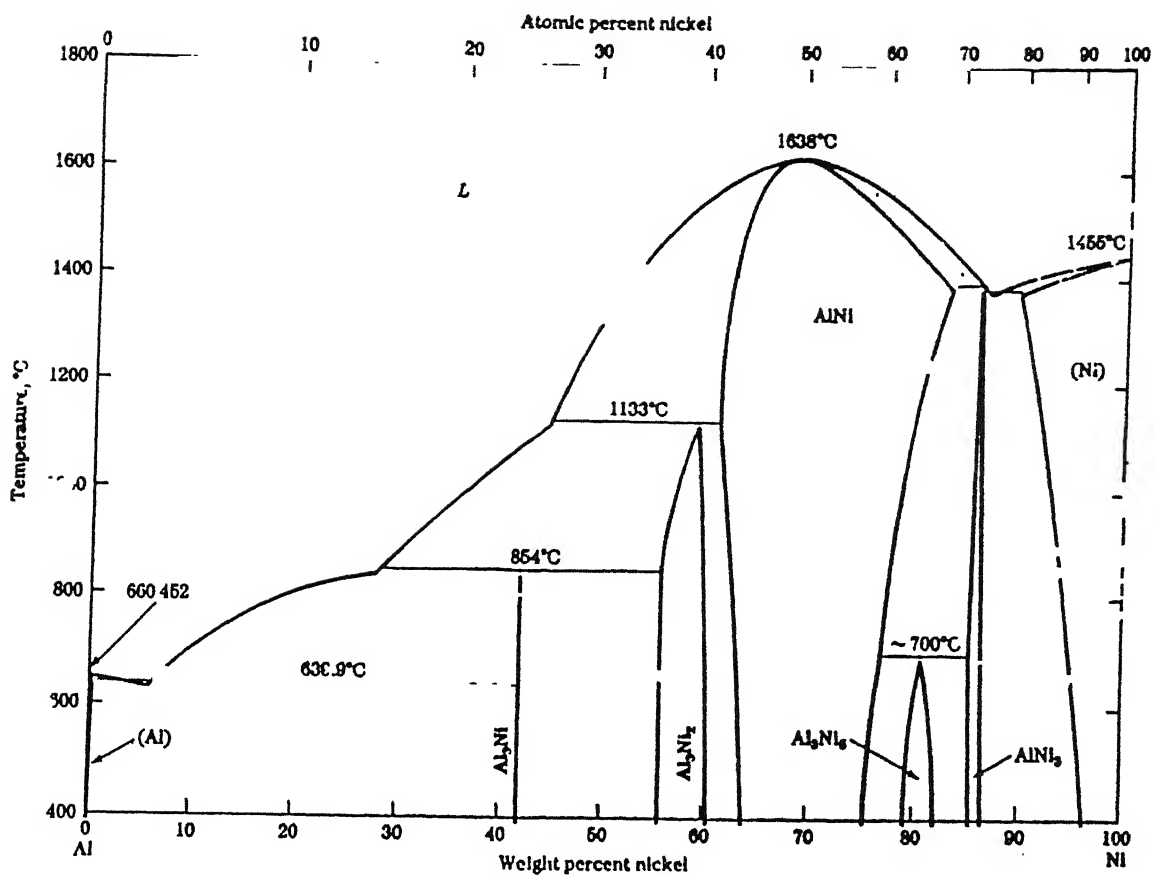
Fig 5.6 Al-Ni Phase diagram
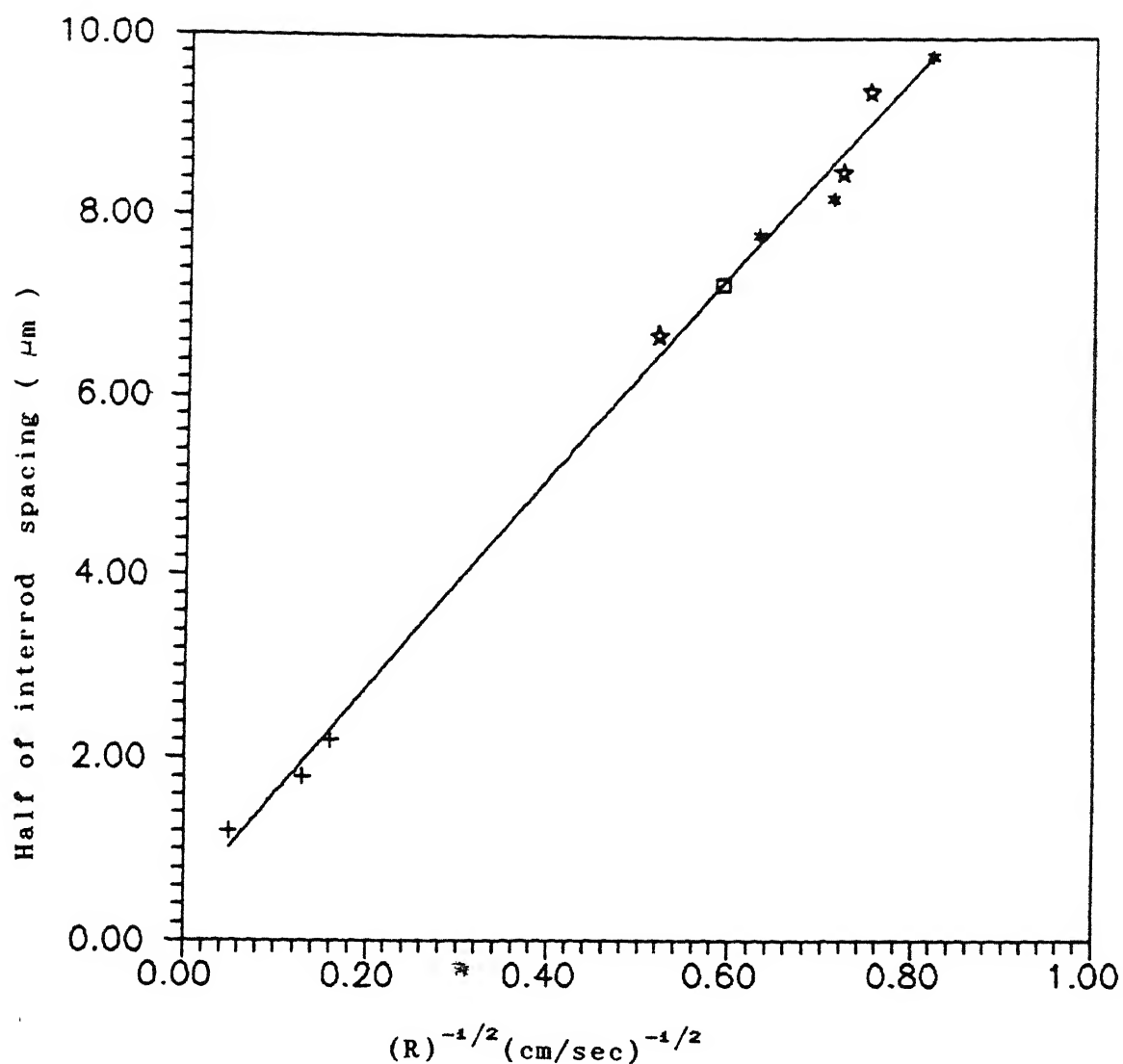
Fig 5.7 Plot of λ vs $R^{-1/2}$

$\square$ Our experimental point

$\star$ Bonde (1974)

$\ast$ Livingston et al.

$+$ Lemkey et al.

Table 5.1 Master alloy composition from gravimetric analysis.

S.No	Concentration of Ni (Wt %)
1	32.51
2	36.98
Average	34.75

Table 5.2 Eutectic alloy composition from SEM.

S.No	Concentration of Ni (Wt %)
1	5.92
2	5.90
Average	5.91

Table 5.3 Solute analysis in longitudinal direction.

Nature of the Section	Distance (μm)	Ni Content in Al_3Ni (β) phase (Wt %)	Ni Content in Al (α) matrix (Wt %)	Ni Content (Wt %)
Directionally Solidified Section	0.0	(A) 39.90	(A') 1.72	--
	262.5	(B) 39.63	(B') 1.16	--
	525.0	(C) 39.21	(C') 1.28	--
	—			
Quenched Section	628.0	--	--	6.20
	828.0	--	--	6.57
	1028.0	--	--	6.50

Fig 5.8 Solute analysis in longitudinal direction.
Solid line - Experimental.
Dotted line - Predicted.

Fig 5.9 Micrograph showing the solute analysis in
longitudinal direction.

39.5 wt% compared to the theoretical value of 42.05 wt%) can be explained as follows. the diameter of β phase rods is approximately 2 to 5 μm (Fig 5.2, 5.3). When the probe was focussed on these β- phase rods for measuring Ni content some of the signal from the adjoining α - phase must have resulted in the observation of a lower Ni concentration.

(5.6) The result of the solute analysis done in transverse direction is shown in table 5.4. It is done ahead of the S-L interface in quenched section at 3μm distance. The above table also contain the values of C_s and C_l calculated from theoretical treatment. The nature of the profile obtained experimentally is simil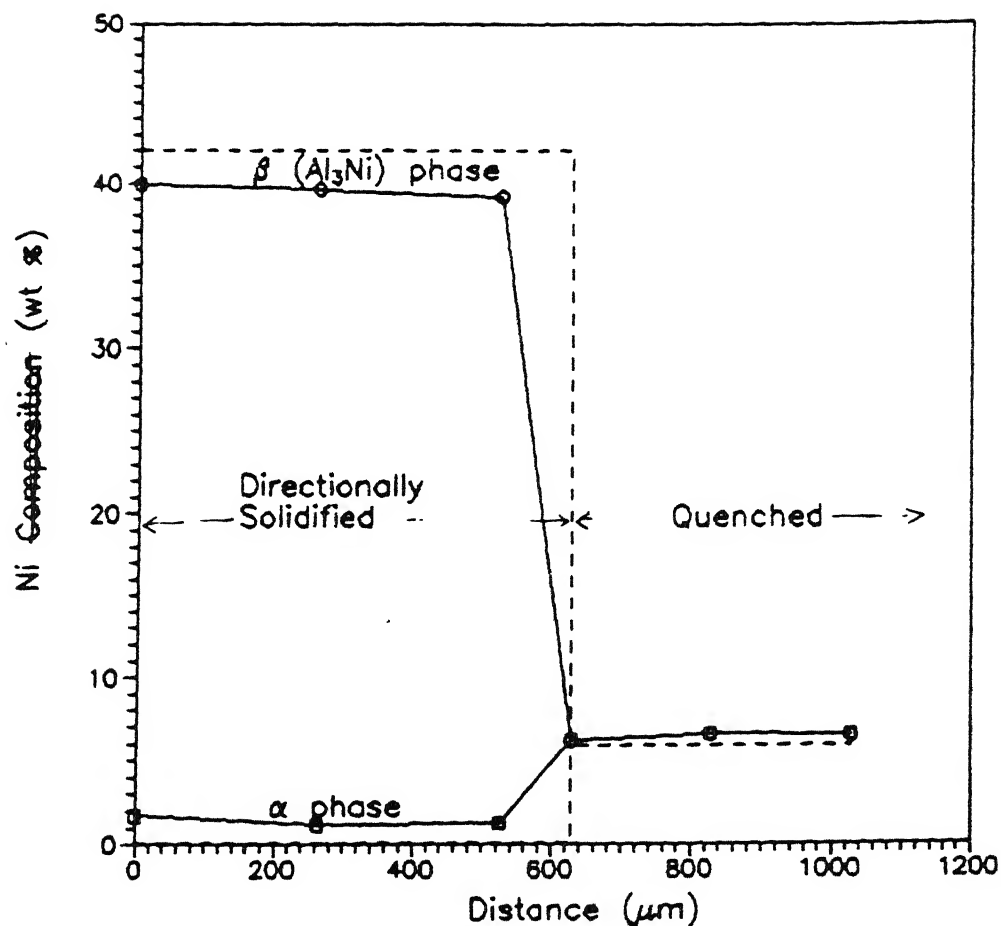ar to that of predicted one. The plot is shown in Fig5.10. The point to point matching of theoretical and experimental C_L values is done by appropriately choosing the D_L values.

The profile obtained in quenched section at 3μm from the interface shown in Fig 5.10 clearly indicates the experimental concentration values match with the predicted values up to about r = 3μm and then they deviate considerably. This difference in prediction of the results could be explained in terms of the Nickle diffusivity and the assumptions made in theoretical model.

The present theoretical model assumes that the interface is planar which also means that the concentration variation in transverse direction (i.e., from leading to lagging part of the β rods) is negligible. This is the assumption which leads to the following boundary conditions to solve the differential equation.

$$\frac{\partial C_L}{\partial z'} \bigg|_{z'=0} = -\frac{R}{D_L} \cdot \left[C_E - C_{\alpha M} \right], \quad S_\beta \leq r \leq S_\alpha + S_\beta$$

Table 5.4 Solute analysis in transverse direction.

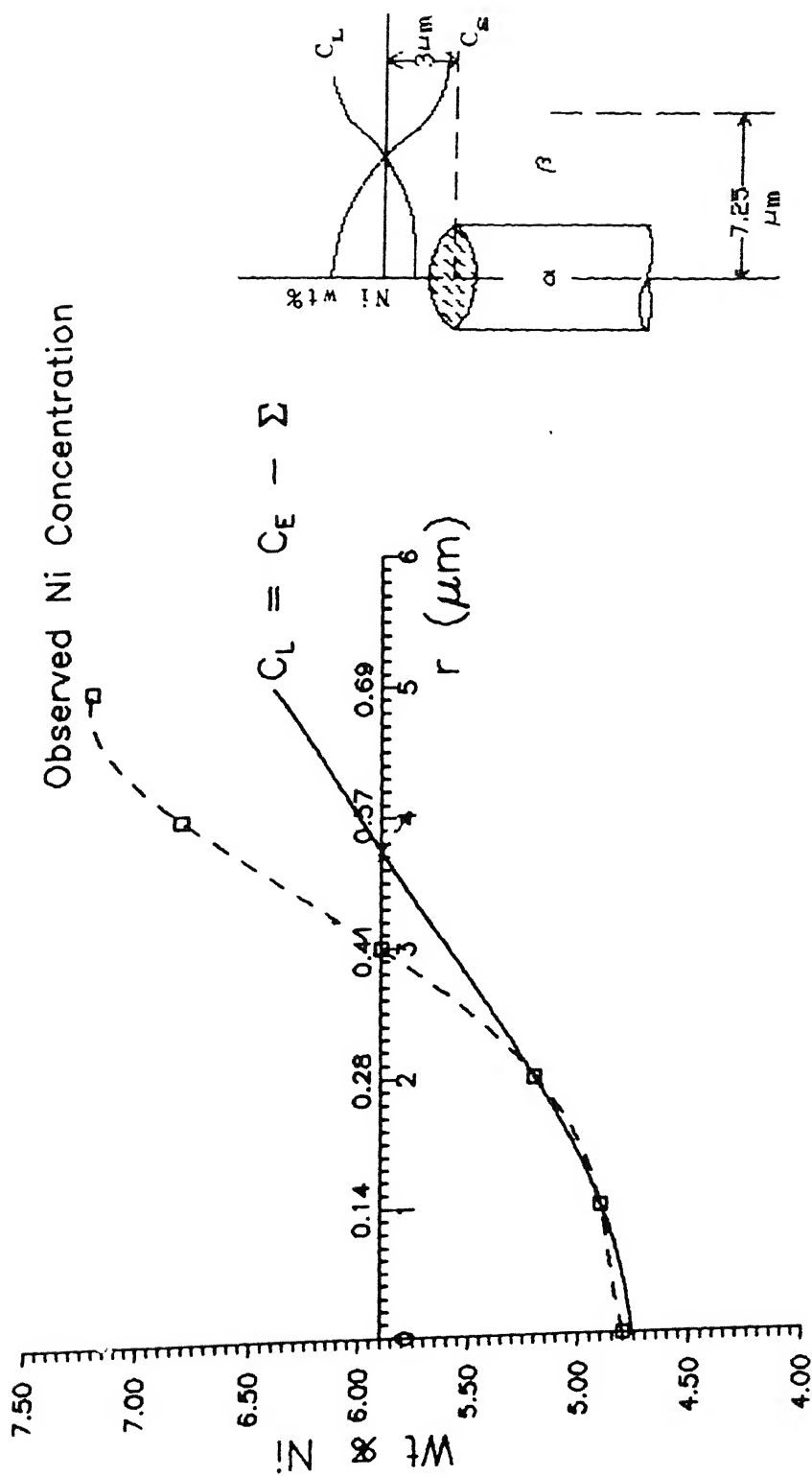| Distance (r) (μm)	($\dfrac{r}{S_\alpha + S_\beta}$)	C_L (Theoritical) Wt % Ni	C_s (Theoritical) Wt % Ni	C_L (Experimental) Wt % Ni
0.0	0.00	4.76	7.13	4.80
1.0	0.14	4.90	6.90	4.90
2.0	0.28	5.20	6.60	5.20
3.0	0.41	5.60	6.20	5.90
4.0	0.57	6.00	5.80	6.80
5.0	0.69	6.39	5.41	7.20

68

Fig 5.10 Solute analysis in transverse direction.
Solid line — predicted.
Dotted line — Experimental.

and,

$$\left.\frac{\partial C_L}{\partial z'}\right|_{z'=0} = -\frac{R}{D_L} \cdot \left[C_E - C_{\beta M}\right], \quad 0 \leq r \leq S_\beta$$

Probably at higher rates of solidification there may be reasonable concentration variations at the interface. Since this fact is not taken care of in the present treatment, this would have lead to difference in predicted and experimental values. This result also gives an indication of the fact that probably the present treatment predicts better results for lower rates of solidification.

(5.7) The values of D_L chosen to match with experimental C_L values is tabulated in table 5.5. The results are plotted in Fig 5.11. The figure shows that the D_L values change from 1.125 $\times$ 10^{-6} Cm^2/sec (at $r = 0\mu m$) to 0.2 $\times$ $10^{-6}Cm^2$/sec (at $r = 5\mu m$).One of the reasons for a change in D_L could be the variations in Nickle concentration in the transverse direction.Further, we have ignored the curvature effects in our theoretical model. Any effects of small impurities present have also not been considered. All these approximations when clubbed as a variation in D_L to match the experimental and theoretical values are resulting in the range of D_L as given here.

(5.8) Microhardness measurements made are plotted and shown in Fig 5.12 and table 5.6 respectively . Micrographs of the indented portions of the sample are shown in Figs 5.13 (a) & 5.13 (b). There is almost two fold increase in hardness as we approach quenched interface from directionally solidified side of the ingot.The hardness of the quenched ingot almost remains constant (~ 112 VHN).The marked increase in hardness can be explained by considering the grain size of the quenched portion.

Table 5.5 Variation of bestfit interface diffusion coefficient (D_L) along transverse direction.

Distance (r) (μm)	D_L X 10^6 (cm^2/sec)
0.0	1.125
1.0	1.125
2.0	1.125
3.0	1.100
4.0	0.900
5.0	0.200
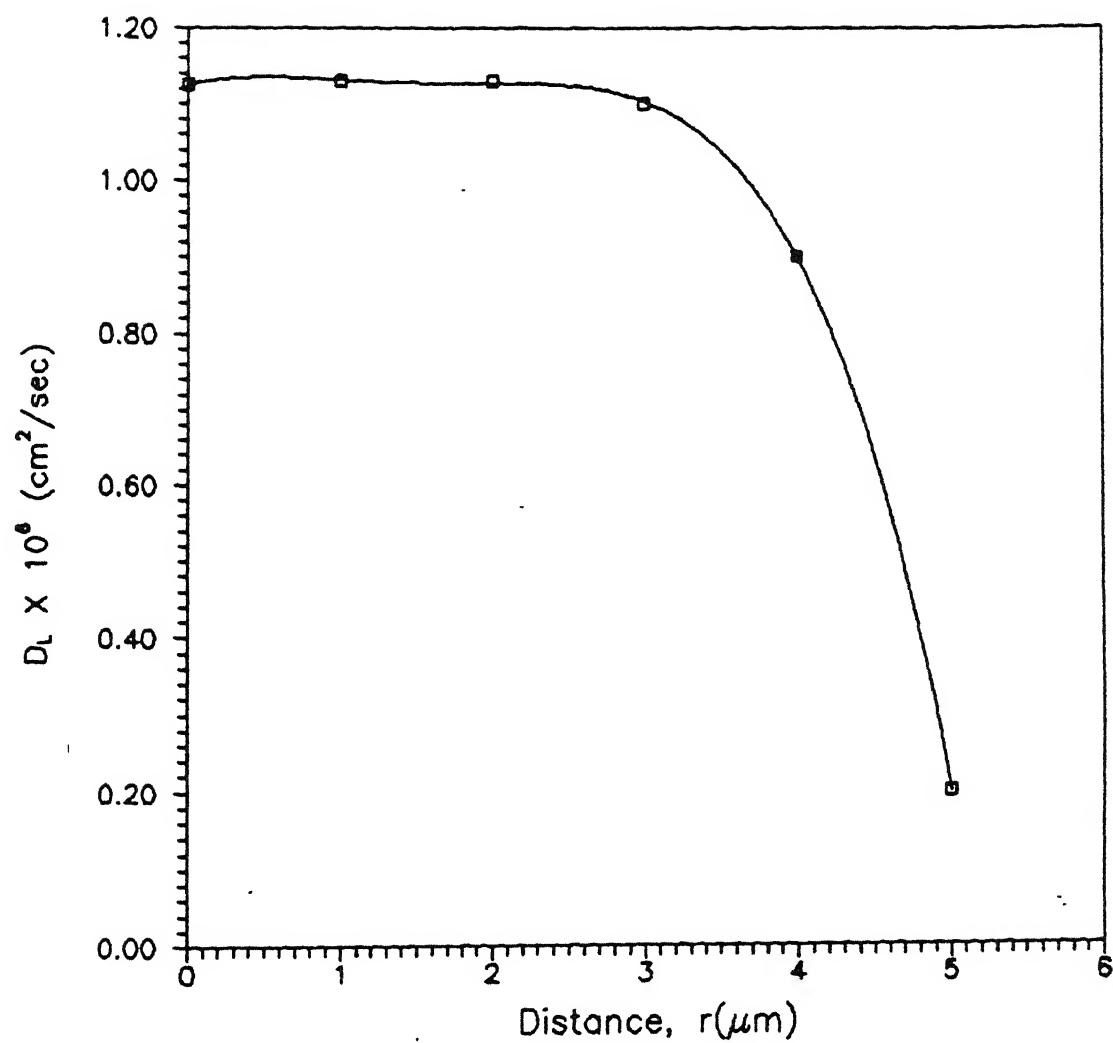
Fig 5.11 Variation of bestfit interface diffusion coefficient (D_L) along the transverse direction.
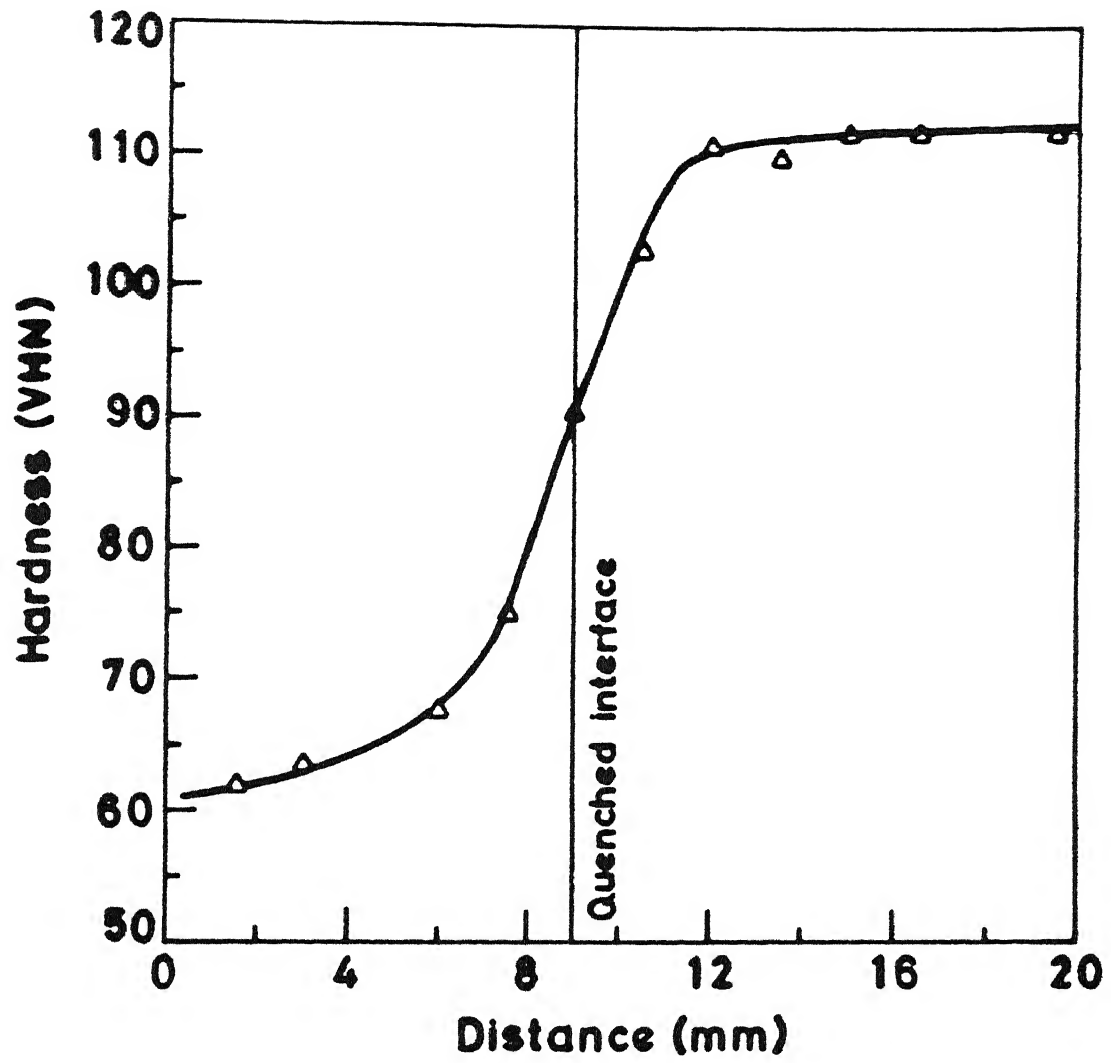
Fig 5.12 Vickers microhardness variation along the length of the ingot containing frozen in interface.

Table 5.6 Vickers microhardness values along the length of the ingot containing frozen in interface.

Distance (mm)	Average Diagonal length of the Indentation (μm)	Hardness (VHN)
1.5	54.70	62.0
3.0	54.00	63.6
6.0	52.30	67.8
7.5	49.70	75.1
9.0	45.25	90.8
10.5	42.50	103.0
12.0	40.90	111.0
13.5	41.15	110.0
15.0	40.75	112.0
16.5	40.75	112.0
19.5	40.65	112.0
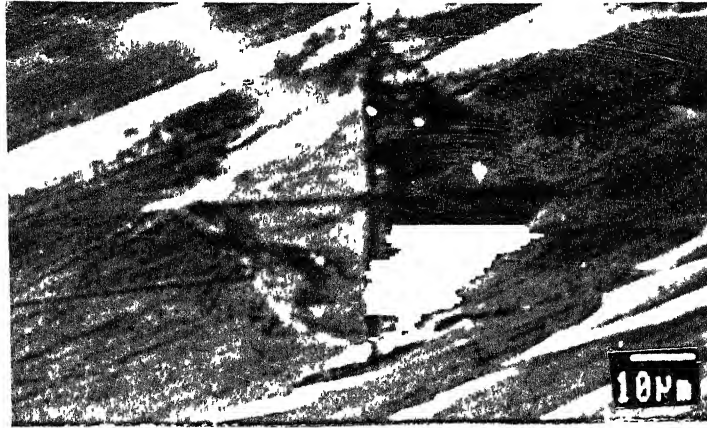
(a)
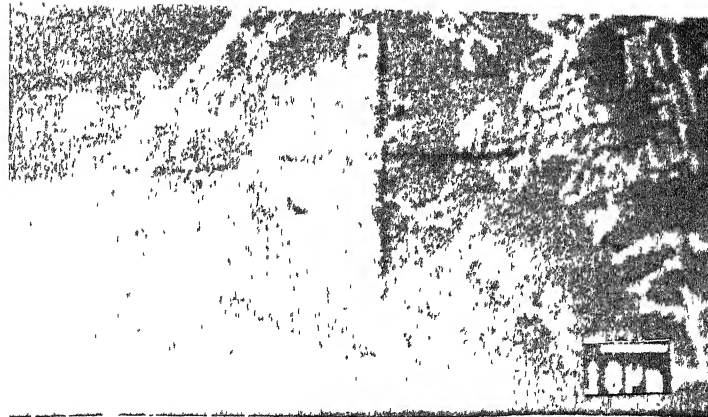
(b)

Fig 5.13 Micrographs of the indented sample.
(a) On directionally solidified section,
(b) On quenched section.

Grain boundaries provide obstacles to dislocation motion. As the orientation of the crystals on either side of the grain boundary is different and random, a dislocation moving on a common slip plane in one crystal can rarely move on to a similar slip plane in the adjacent crystal. In addition, the crystals are separated by a thin non-crystalline region,which is the characteristic of a large angle grain boundary. Hence dislocations are stopped by a grain boundary and pile up against it.The smaller is the grain size, the more frequent is the pile up and hence higher the tensile strength and hardness. Since quenched section has much finer grains compared to directionally solidified section,we observe the difference in hardness.

The increase in hardness could also be attributed to solid solution strengthening. As the quenched ingot would retain excess of Nickle in the Aluminium matrix the stress fields around the Nickle atoms could possibly interact with the stress fields of the dislocations there by hindering their movement.

(5.9) Spot analysis done on the top most portion of the quenched ingot(i.e. the part of the ingot which first came in contact with LN_2 during quenching) revealed the existence of number of finely distributed Al-Ni intermetallics for example some with Nickle compositions 32.42 wt% & 27.9 wt% corresponding to the molecular formulae Al_2Ni,Al_5Ni_2 respectively.The Al_2Ni belongs to the family of Laue phases. The existence of these phases has not been reported in the Al-Ni system so far. The Al_2Ni phase could have an FCC structure with all the lattice points occupied by Al atoms and Ni atoms at four alternate cube edges and the

cube centre.The Ni atom positions correspond to the octahedral sides of the FCC lattice.

The Ni atoms are chosen to be located at the alternate cube edges because this seems to be the lowest energy arrangement possible.The Al_5Ni_2 phase probably has a very complicated crystal structure.

(5.10) LAUE BACK REFLECTION PIN HOLE PATTERN:

Laue back reflection analysis done on quenched section (shown in Fig 5.14) revealed the existence of coarser grains in contrast to finer grains which is expected.This means that the size of the grain must be larger than the X-ray beam diameter used for back reflection analysis. The beam diameter used is 10 μm microns where as the grain size found is 15 μm. The micrograph showing the grains is shown in Fig 5.15

The Laue back reflection pattern obtained has discreet spots(done on quenched section), there is no evidence of concentric rings which is expected for a fine grained system. This lead to the conclusion that the quenched section has larger grains than the X-ray beam diameter.
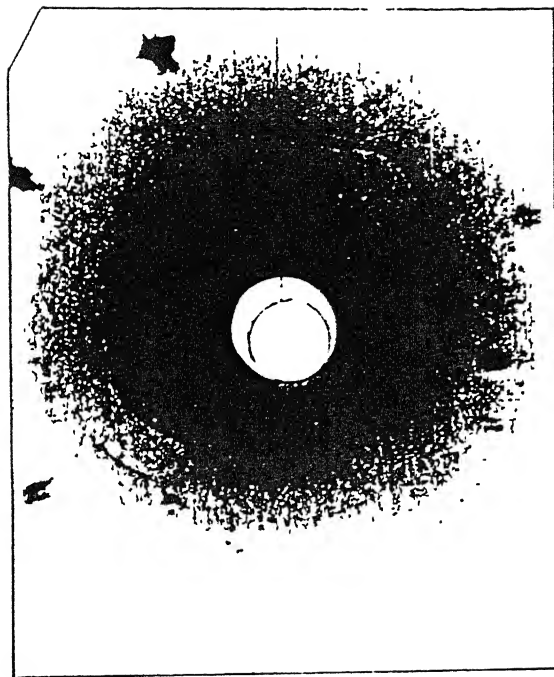
Fig 5.14 Laue pattern On quenched section.

Fig 5.15 Micrograph of the quenched section showing the grains. (X 2000)

CONCLUSIONS

1. Directional solidification of Al – 5.7 wt% Ni eutectic alloy at $R = 7.9 \times 10^{-4}$ cm/sec and $G = 25°c/cm$ leads to interrod spacing of 14.5 μm, which fits very well on the extended plot of interrod spacing Vs growth rate obtained by earlier workers for the same system.

2. Laue back reflection pin hole patterns and also metallography for both directionally solidified and quenched sections show the presence of coarse, near single crystal grains.

3. The hardness measures about two fold increase in the quenched section compared to the directionally solidified section and the hardness variation at the interface is not as steep as one may expect if the solid – liquid interface were to be sharp.

4. Solute distribution profile obtained in the longitudinal direction is similar to the expected one with α – matrix having excess of Ni and β – rods having lower Ni content, but with a overall conservation of solute distribution around the β rods.

5. Solute distribution profile in the transverse direction at 3 μm in to the quenched section is similar to the predicted profile up to $r = 3$ μm and later it deviated considerably.

6. Matching of experimental and theoretical concentration profiles indicates the variation in D_L values in transverse direction ahead of the β – rod.

CALCULATIONS

The complete solution that satisfies the differential equation

$$\frac{\partial^2 C_L}{\partial r^2} + \frac{1}{r} \cdot \frac{\partial C_L}{\partial r} + \frac{\partial^2 C_L}{\partial z'^2} + \frac{R}{D_L} \cdot \frac{\partial C_L}{\partial z'} = 0 \quad \text{is}$$

$$C_L = C_E - \sum_{1=1}^{\infty} A_1 \mathrm{Exp} \left[-\frac{a}{2} \left\{ 1 + \sqrt{1 + \frac{4K_1^2}{a^2}} \right\} \delta z' \right] J_0(K_L \delta r)$$

where,

$$A_1 = \frac{4 \left[C_{\beta M} - C_{\alpha M} \right]}{\left\{ 1 + \sqrt{1 + \frac{4K_1^2}{a^2}} \right\}} \cdot \frac{J_1(K_1 \cdot \delta S_\beta)}{K_1 \left[J_0(K_1) \right]}$$

For the evaluation of A_1, C_L the variables having the following values are used

$$C_{\alpha M} = 0.05 \text{ Wt\% Ni,}$$

$$C_{\beta M} = 42.05 \text{ Wt\% Ni,}$$

$$C_E = 5.9 \text{ Wt\% Ni,}$$

$$R = 7.9 \times 10^{-4} \text{ cm/sec,}$$

$$z' = 3 \ \mu m,$$

$$S_\alpha + S_\beta = 7.25 \times 10^{-4} \text{ cm/sec.}$$

Evaluation of 'a':

The values of 'a' evaluated for different D_L used in the present analysis are tabulated below;

$D_L \times 10^6 (cm^2/sec)$	a
1.125	0.46
1.100	0.52
0.900	0.66
0.200	2.86

Evaluation of $J_0(k_1)$ and $\langle J_0(k_1)\rangle^2$

The values evaluated are tabulated below [40]

l	k_1	$J_0(K_1)$	$\langle J_0(K_1)\rangle^2$
1	3.832	−0.403	0.162
2	7.016	0.300	0.090
3	1 0.173	−0.275	0.076

Evaluation of $J_1(K_1 \delta S_\beta)$

The values are tabulated below

l	$k_1 \delta S_\beta$	$J_1(k_1 \delta S_\beta)$
1	0.651	0.308
2	1.193	0.496
3	1.729	0.579

Evaluation of $J_0(k_1 \delta r)$

The values of $J_0(k_1 \delta r)$ calculated are,

l	J_0 $\delta r=0$	J_0 $\delta r=0.14$	J_0 $\delta r=0.28$	J_0 $\delta r=0.41$	J_0 $\delta r=0.55$	J_0 $\delta r=0.61$
1	1	0.93	0.73	0.47	0.16	−0.12
2	1	0.77	0.25	−0.22	−0.40	−0.23
3	1	0.56	−0.21	−0.38	0.03	−0.03

Evaluation of A_1

The values of A_1 evaluated for different values of 'a' are tabulated below;

a	A_1	A_2	A_3
0.46	4.71	4.20	2.78
0.52	5.29	4.72	3.13
0.66	7.15	6.45	4.30
2.86	21.62	22.02	15.38

Evaluation of C_L (Specimen calculation)

A specimen calculation is shown below for 'a' = 0.46 and δr = 0.14

$$C_L = 5.9 - 4.71 Exp\{-0.23[17.69]0.41\}0.93$$
$$- 4.20 Exp\{-0.23[31.52]0.41\}0.77$$
$$- 2.78 Exp\{-0.23[45.24]0.41\}0.56$$

$$= 4.9$$

The values of C_L as calculated above are tabulated in the following table

r	δr	C_L
0	0	4.76
1	0.14	4.90
2	0.28	5.20
3	0.41	5.60
4	0.57	6.00
5	0.69	6.39

(1) J.L.Walter and H.E.Cline, Met.Trans., 1, 1970, 1226.

(2) F.L.Versnyder and M.E.Shank, Mat.Sci.and Engg., 6, 1970, 246.

(3) C.H.Hund, Foundry Trade Journal, 128, 1970, 815.

(4) F.D.Lemkey and M.J.Salkind in H.S.Peiser(Ed.),"Crystal Growth", p.171, Pergamon, Oxford, 1967.

(5) F.S.Glasso, J.Metals, 19, 1967, 17.

(6) W.Albers and J.verberkt, J.Material Science, 7, 1970,249.

(7) P.R.Sahm and M.O.Speidl(Ed.),"High Temperature Materials in Turbine Blades",Elsevier Scientific PublishingCo.,Amsterdam, 1974, 79.

(8) J.D.Hunt and K.A.Jackson, Trans.AIME., 236, 1966, 843.

(9)G.J.Davies, "Solidification and Casting", Applied Science Publishers Ltd., London, 1973.

(10)M.G.Day and A.Hellawell, Proc. of Royal Society, A.305, 1963, 473.

(11) J.D.Hunt and K.A.Jackson, Trans.AIME., 236, 1966, 1129.

(12) W.A.Tiller, "Polyphase Solidification",Seminar on Liquid Metals and Solidification, ASM., Cleaveland, Ohio.

(13) M.Flemings, Trans.AIME., 239, 1967, 1534.

(14) M.Tassa and J.D.Hunt, "The measurements of Al-Cu dendrite tip and eutetic interface temperatures and their use for predicting the extent of eutetic range", J.Cryst.Growth, 34, 1976, 38.

(15) S.M.D.Borland and R.Elliott, "Growth temperatures in $Al-CuAl_2$ and Sn-Cd eutetic alloys", Met.trans.AIME., 9A, 1978, 1068.

(16) R.M.Jordan and J.D.Hunt, "The growth of lamellar eutetic structures in the Pb-Sn and Al-CuAl$_2$ systems", Met.Trans.AIME., 2, 1971, 3401.

(17) F.D.Lemkey, R.W.Hertzberg and J.A.Ford, Trans.AIME., 233, 1965, 334.

(18) J.D.Livingston, H.E.Cline, E.F.Keck and R.R.Russel, "High speed solidification of several eutectic alloys",General electric Co., Schenectady, N.Y., G.E.Rept. 69-c-328.

(19) G.A.Chadwick, J.Inst.Metals, 18, 1963-1964, 92.

(20) V.L.Davies, J.Inst.Metals, 10, 1964-1965, 93.

(21) F.R.Mollard and M.C.Flemings,Trans.AIME.,239, 1967, 1534.

(22) K.A.Jackson and J.D.Hunt, Trans. AIME., 236, 1966, 1129.

(23) B.Chalmers, "Principles of solidification", John Wiley Sons, Inc., Newyork, 1964.

(24) J.D.Hunt and K.A.Jackson, Trans. AIME., 236, 1966, 843.

(25) J.D.Hunt and D.T.J.Hurle, Trans. AIME., 242, 1968, 1043.

(26) C.J.Davidson, I.O.Smith and G.A.Chadwick, "Effect of heat treatment and interlamellar spacing on the tensile deformation of the aligned Al-CuAl$_2$ eutectic", 28, 1980, 61.

(27) B.J.Shaw, "Room temperature mechanical properties of Cd-Zn lamellar eutectic alloys", Acta Met., 15, 1967, 1169.

(28) S.F.Dirnfled, D.Schechtman and J.Mironi, "The micro structure and mechanical properties of directionally solidified Ni-Sn eutectic alloy", Mat.Sci. andEngg., 68, 1984-'85, 183.

(29) F.S.J.Jabzynski and B.Cantor, "The solidification and mechanical properties of chill cast Al-Al$_3$Ni and Cu-Al$_2$Cu eutectic alloys", J.Mat.Sci., 16, 1981, 2269.

(30) Horishikato and J.R.Cahoon, "Tensile properties of directionally solidified Al-4Wt% Cu alloys with columnar and equiaxed grains", Met.Trans.A, 17A, 1986, 823.

(31) E.Bulluck and M.Mc Lean, "Effect of variations in growth rate and temperature gradient on microstructure and creep properties of directionally solidified eutectic alloys", Met.Trans.A, 17A, 1982, 715.

(32) F.L.Versnyder and Shank, Mat.Sci.and Engg., 6, 1970, 213.

(33) J.Liu, Y.Y.Lee and Z.Q.Hu, "Effect of directional solidification on resistance to Hydrogen embrittlement of a stainless steel", Mat.Sci.and Engg., A117, 1989, 221.

(34) D.C.Houghton and Jones, "The thermal stabilities of in-situ composites in a temperature gradient: the $Al-Al_3Ni$ and Cu-Cr eutectics", Acta.Met., 27, 1979, 1031.

(35) H.B.Smartt, Tu and T.H.Courtney, "Elevated temperature stability of $Al-Al_3Ni$ eutectic composite", Met.Trans.AIME., 2, 1971, 2717.

(36)A.J.Ardell,"Isotropic fibre coarsening in unidirectionally solidified eutectic alloys", Met.Trans.AIME., 3, 1972, 1395.

(37) E.C.Stoner and E.P.Wohlfahrt, Phil.Trans.Roy.Soc., London, A240, 1948, 599.

(38) J.D.Livingston, J.Appl.Phys., 38, 1967, 2408.

(39) M.N.Shetty, D.K.Rawat and K.N.Rai, "Magnetic properties of directionally solidified Bi-Mn alloys", J.Mat.Sci., 22, 1987, 1908.

(40) Arnold N. Lowan,"Tables of the Bessel functions $J_0(Z)$ and $J_1(Z)$ for complex arguements", Columbia University press, Newyork, 1947.

(41)F.B.Hilderbrand,"Advanced calculus for applications", Printice-Hall, Inc., 1962.

APPENDIX

Boundary condition (1): $C_L(r,z')\Big|_{z'=} = C_E$ gives;

$$C_L = C_E + \sum_{l=1}^{\infty} A_l \, \mathrm{Exp}\left[-\frac{a}{2}\left\{ 1 + \sqrt{1 + \frac{4 \, Kl^2}{a^2}} \right\}\delta z \right] J_0(k_l \delta r) \tag{A1}$$

Boundary condition(2): $\dfrac{\partial C_L}{\partial r}\Big|_{r=0} = 0$ is automatically satisfied because,

$$\frac{\partial J_0(k_l \delta r)}{\partial r}\Bigg|_{r=0} = -\,\delta k_l J_1(k_l \delta r)\Bigg|_{r=0} = 0 \tag{A2}$$

Boundary condition (3):

$$\frac{\partial C_L}{\partial r}\Bigg|_{r = S_\beta + S_\alpha} = 0, \qquad \text{gives,}$$

$$\sum_{l=1}^{\infty} A_l \, \mathrm{Exp}\left[-\frac{a}{2}\left\{ 1 + \sqrt{1 + \frac{4 \, Kl^2}{a^2}} \right\}\delta z \right]\cdot\left[\delta \, k_l J_1(k_l') \right] = 0 \tag{A3}$$

For a non zero solutuon, we have to set $J(k_1) = 0$, the roots of which will determine the k_l. Some values of K_l for which $J_1(k_1) = 0$ are tabulated below [41]:

l	k_1
1	3.832
2	7.016
3	10.173
4	13.323
5	16.470

In dimensionless coordinates,

$$\frac{\partial C_L}{\partial Z'} = \delta \frac{\partial C_L}{\partial Z'}.$$

The boundary conditions (4),(5) then become;

$$\delta \frac{\partial C_L}{\partial Z*}\bigg|_{Z' = 0} = -\frac{R}{D_L} \cdot \left[C_E - C_{\alpha M} \right] \qquad (A4)$$

$$\delta S_\beta \leq r^* \leq 1$$

$$\delta \frac{\partial C_L}{\partial Z*}\bigg|_{Z* = 0} = -\frac{R}{D_L} \cdot \left[C_E - C_{\beta M} \right] \qquad (A5)$$

$$0 \leq r* \leq \delta S_\beta$$

The LHS of A4 and A5 is;

$$= \sum B_1 \, J_0(k_1 r*) \qquad (A6)$$

Where,

$$B_1 = -\frac{\delta a}{2} \left\{ 1 + \sqrt{1 + \frac{4 K_l^2}{a^2}} \right\} A_1 \qquad (A7)$$

and,

$$\therefore \quad A_1 = -\frac{B_1}{-\dfrac{\delta a}{2} \left\{ 1 + \sqrt{1 + \dfrac{4 K_l^2}{a^2}} \right\}} \qquad (A8)$$

The constants B_1 are determined by using the property of the Bessel functions that they are orthogonal with respect to a weight function in a suitable interval. In this case the weight function is r^* it self and the interval is 0 to 1. The boundary conditions (4) and (5) yield;

$$B_1 \int_0^1 r* \left[J_0(k_1 r*) \right] dr* = -\frac{R}{D_L} \left[C_E - C_{\beta M} \right] \int_0^{\delta S_\beta} r* J_0(k_1 r*) dr*$$

$$-\frac{R}{D_L} \left[C_E - C_{\alpha M} \right] \int_{\delta S_\beta}^1 r* J_0(k_1 r*) dr* \tag{A9}$$

When the condition $J_0(k_1) = 0$ is satisfied as in A3 above, then,

$$B_1 \int_0^1 r* \left[J_0(k_1 r*) \right] dr* = B_1 \left[J_0(k_1) \right]^2 / 2 \tag{A10}$$

The RHS of A9 & A10 integrates to

$$-\frac{R}{D_L} \cdot \left[C_{\beta M} - C_{\alpha M} \right] \frac{J_1(K_1 \delta S_\beta)}{k_1} \tag{A11}$$

$$\therefore \quad B_1 = \frac{2R}{D_L} \cdot \left[C_{\beta M} - C_{\alpha M} \right] \frac{J_1(K_1 \delta S_\beta)}{k_1 \left[J_0(k_1) \right]^2} \tag{A12}$$

And from A8,

$$A_1 = -\frac{4 \left[C_{\beta M} - C_{\alpha M} \right]}{\left[1 + \sqrt{1 + \frac{4k\iota^2}{a^2}} \right]} \cdot \frac{J_1(k_1 \delta S_\beta)}{k_1 \left[J_0(k_1) \right]^2} \tag{A13}$$

The complete solution is,

$$C_L = C_E - \sum_{1=1}^{\infty} A_1 \cdot \mathrm{Exp} \left[-\frac{a}{2} \left\{ 1 + \sqrt{1 + \frac{4k\iota^2}{a^2}} \right\} \delta z' \right] J_0(k_1 \delta r) \tag{A14}$$

When, $\dfrac{k_1}{a} \gg 1$, $1 + \sqrt{1 + \frac{4k\iota^2}{a^2}} \cong \frac{2k\iota}{a}$, the solution reduces to;

$$C_L = C_E - \sum_{1=1}^{\infty} 2a \left[C_{\beta M} - C_{\alpha M} \right] \cdot \frac{J_1(k_1 \delta S_\beta)}{k_1^2 \left[J_0(K_1) \right]} \cdot \mathrm{Exp} \left[-k_1 \delta z' \right] \cdot J_0(k_1 \delta r) \tag{A15}$$

Where, $a = \dfrac{R}{D_L}$.